

Further Evidence of Modified Spin-down in Sun-like Stars: Pile-ups in the Temperature–Period Distribution

TREVOR J. DAVID ,^{1,2} RUTH ANGUS ,^{2,1,3} JASON L. CURTIS ,³ JENNIFER L. VAN SADERS ,⁴ ISABEL L. COLMAN ,² GABRIELLA CONTARDO ,¹ YUXI LU ,^{3,2} AND JOEL C. ZINN 

¹Center for Computational Astrophysics, Flatiron Institute, New York, NY 10010, USA

²Department of Astrophysics, American Museum of Natural History, Central Park West at 79th Street, New York, NY 10024, USA

³Department of Astronomy, Columbia University, 550 West 120th Street, New York, NY, USA

⁴Institute for Astronomy, University of Hawai'i, Honolulu, HI, USA

(Received February 4, 2022; Revised March 17, 2022)

ABSTRACT

We combine stellar surface rotation periods determined from NASA’s Kepler mission with spectroscopic temperatures to demonstrate the existence of pile-ups at the long-period and short-period edges of the temperature–period distribution for main-sequence stars with temperatures exceeding \sim 5500 K. The long-period pile-up is well-described by a curve of constant Rossby number, with a critical value of $R_{\text{Ocrit}} \lesssim 2$. The long-period pile-up was predicted by van Saders et al. (2019) as a consequence of weakened magnetic braking, in which wind-driven angular momentum losses cease once stars reach a critical Rossby number. Stars in the long-period pile-up are found to have a wide range of ages (\sim 2–6 Gyr), meaning that, along the pile-up, rotation period is strongly predictive of a star’s surface temperature but weakly predictive of its age. The short-period pile-up, which is also well-described by a curve of constant Rossby number, is not a prediction of the weakened magnetic braking hypothesis but may instead be related to a phase of slowed surface spin-down due to core–envelope coupling. The same mechanism was proposed by Curtis et al. (2020) to explain the overlapping rotation sequences of low-mass members of differently aged open clusters. The relative dearth of stars with intermediate rotation periods between the short- and long-period pile-ups is also well-described by a curve of constant Rossby number, which aligns with the period gap initially discovered by McQuillan et al. (2013a) in M-type stars. These observations provide further support for the hypothesis that the period gap is due to stellar astrophysics, rather than a non-uniform star-formation history in the Kepler field.



Keywords: Stellar rotation (1629) — Solar analogs (1941) — Stellar evolution (1599) — Stellar magnetic fields (1610) — Stellar winds (1636)

1. INTRODUCTION

Solar-type and low-mass stars ($M \lesssim 1.3 M_{\odot}$) lose mass and angular momentum through magnetized winds (Parker 1958; Weber & Davis 1967; Mestel 1968; Kawaler 1988). Consequently, stellar rotation rates are observed to decline with age. Skumanich (1972) presented the first attempt to calibrate this age-rotation relationship using the rotation periods of Sun-like stars

in open clusters with independently determined ages, finding a $P_{\text{rot}} \propto t^{1/2}$ scaling, where t is stellar age. In the intervening decades, observational determinations of stellar rotation periods among open cluster members revealed how stellar spin rates evolve in more detail, leading to the calibration of the so-called gyrochronology method (Barnes 2003, 2007, 2010; Mamajek & Hillenbrand 2008; Meibom et al. 2009).

The arrival of continuous, high-precision, long-baseline photometry from NASA’s Kepler space telescope (Borucki et al. 2010) provided a watershed moment for stellar rotation studies, yielding period detections for tens of thousands of stars (e.g. Reinhold et al.

Corresponding author: Trevor J. David
tdavid@flatironinstitute.org

2013; McQuillan et al. 2014; Santos et al. 2021) and allowing for gyrochronology to be extended to older ages (e.g. Meibom et al. 2011, 2015). NASA’s subsequent K2 (Howell et al. 2014) and TESS (Ricker et al. 2015) missions propelled the field of stellar rotation further still, providing an exquisitely detailed picture of how spin rates evolve for stars with a broad range of masses and ages in stellar associations (e.g. Douglas et al. 2016, 2017, 2019; Rebull et al. 2016, 2017, 2018, 2020; Curtis et al. 2019a,b, 2020). New and evermore precise data is becoming available at a rate that is outpacing efforts to re-calibrate gyrochronology, which is necessary to capture the complex relationship between a star’s spin and its age.

For example, efforts to calibrate gyrochronology relations using Kepler asteroseismic targets revealed tension with relations calibrated to open clusters and found that rotation periods could not be described by a single power-law relation with age (Angus et al. 2015). This tension, at least in part, is due to the fact that standard gyrochronology models are unable to account for the anomalously rapid rotation rates of stars older than the Sun, leading to the suggestion that stars with Rossby numbers of $Ro > 2$ experience a phase of weakened magnetic braking (WMB, van Saders et al. 2016).

Forward modeling simulations of the observed Kepler rotation period distribution also provided support for the WMB hypothesis over standard spin-down models, in that WMB models are better able to match the observed long-period edge (van Saders et al. 2019). Those authors also predicted a pile-up of stars along the long-period edge, which they hypothesized could not be seen in the McQuillan et al. (2014) sample due to large errors on T_{eff} in the revised Kepler Input Catalog (KIC, Huber et al. 2014). While van Saders et al. (2019) favored the WMB hypothesis to explain observations, those authors were also careful to point out that a long-period edge can be caused by detection biases, as stars with longer rotation periods (and larger Rossby numbers) have smaller amplitude variations which pose more difficulty to period-detection algorithms.

More recently, Hall et al. (2021) used the asteroseismic rotation rates of Kepler dwarfs, with different selection and detection biases¹ from the van Saders et al. (2019) study and the present work, to argue support for the WMB model. Masuda et al. (2021) also found support for the WMB hypothesis from inference of the rotation period distribution of Sun-like stars using stellar radii

and projected rotational velocities. While the physics responsible for the weakened magnetic braking of solar-type stars is unknown, one hypothesis is that the declining efficiency of wind-driven angular momentum loss is connected to the magnetic field complexity, which may vary with Rossby number (e.g. Réville et al. 2015; van Saders et al. 2016; Garraffo et al. 2016; Metcalfe et al. 2016, 2019).

Here we examine the rotation period distribution of main-sequence stars observed by Kepler, leveraging the recent release of precise spectroscopic parameters from large-scale surveys, to demonstrate the existence of pile-ups at the long- and short-period edges of the $T_{\text{eff}} - P_{\text{rot}}$ distribution of solar-type stars. We discuss our sample in §2, describe the steps of our analysis in §3, discuss some implications of these results in §4, and present our conclusions in §5.

2. SAMPLE SELECTION

Below, we describe the samples utilized in this work. All stars characterized here were targets of NASA’s Kepler mission (Borucki et al. 2010) and have published rotation periods derived from the Kepler data. For each subsample of the Kepler field described below, we combined published rotation periods from a variety of literature sources with spectroscopic parameters provided by large-scale surveys (**Figure 1**).

2.1. California–Kepler Survey

The CKS project gathered high-resolution spectroscopy for 1305 Kepler planet host stars (Petigura et al. 2017). CKS spectra were acquired with the Keck/HIRES spectrograph (Vogt et al. 1994) and spectroscopic parameters were determined by averaging parameters from the SpecMatch pipeline (Petigura 2015) and SME@XSEDE, a Python implementation of the Spectroscopy Made Easy pipeline (Valenti & Piskunov 1996). The internal (relative) errors on T_{eff} from the CKS catalog are estimated at ± 60 K, with systematic errors of ± 100 K estimated from comparison to other catalogs (see Table 7 of Petigura et al. 2017). The metallicity distribution of the CKS sample is centered near solar, with a mean and standard deviation of +0.03 dex and 0.18 dex, respectively.

We compiled rotation periods for these stars from a variety of literature sources including McQuillan et al. (2013b); Mazeh et al. (2015) and Angus et al. (2018). For each star in the sample we then visually inspected the Kepler light curve folded on all available literature periods, as well as the first harmonics and sub-harmonics of those periods, and recorded our preferred period along with a reliability flag. Our procedure is explained in detail in §2.1 of David et al. (2021), and rotation period

¹ Only 48/91 stars in the Hall et al. (2021) sample had rotation periods that were also detected from rotational brightness modulations.

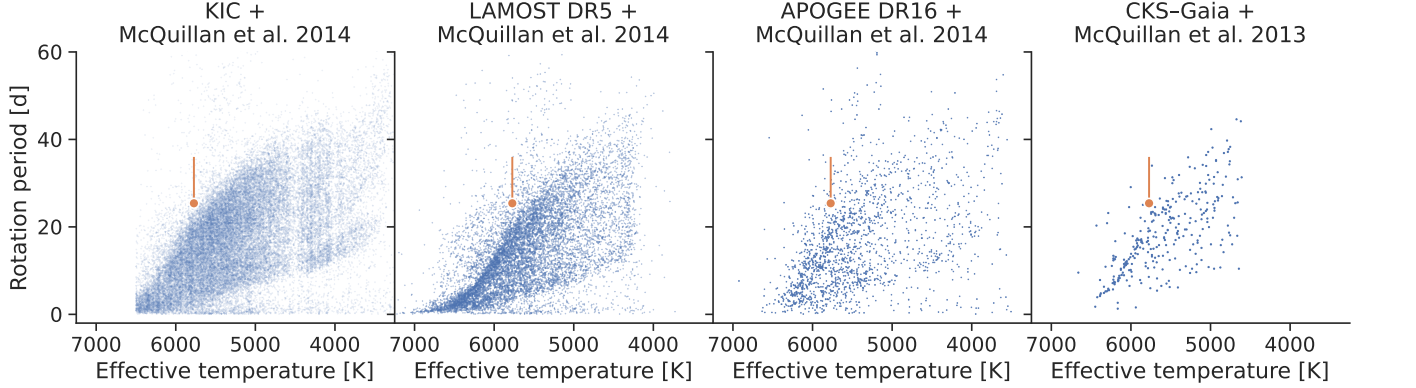


Figure 1. The $T_{\text{eff}}-P_{\text{rot}}$ plane using rotation periods from McQuillan et al. (2014) or, in the case of the CKS sample, McQuillan et al. (2013b) which applied an identical analysis to Kepler Objects of Interest (KOIs), with T_{eff} originating from the source denoted at top. The McQuillan et al. (2014) T_{eff} values originate from the Kepler Input Catalog (KIC, Brown et al. 2011) or Dressing & Charbonneau (2013) for low-mass stars. The orange point in each panel indicates the Sun’s equatorial rotation period, with the errorbar capturing the range of periods measured from the differentially rotating surface. Many of the stars above the long-period pile-up are subgiants which have experienced spin-down due to expansion off the main-sequence, as pointed out in van Saders et al. (2019).

vetting sheets for each Kepler Object of Interest (KOI) are publicly available through Zenodo.² The vast majority of stars in the CKS sample host small planets ($R_P < 4 R_{\oplus}$) and as such it is not expected that the host stars have experienced tidal spin-up from the planets.

In addition to the original CKS catalog, we also cross-matched our sample with the catalogs of Brewer & Fischer (2018) and Martinez et al. (2019), both of which presented spectroscopic parameters for CKS stars based on independent analysis of the same spectra. The Brewer & Fischer (2018) study, referred to here as SPOCS, also published elemental abundances and ages from isochrone fitting for the CKS sample. We additionally cross-matched the CKS catalog with the **LAMOST DR5** catalog (Xiang et al. 2019) which is described further in §2.2. We compare the $T_{\text{eff}}-P_{\text{rot}}$ distributions of the CKS sample using T_{eff} and rotation periods from a variety of sources in Appendix A.

2.2. LAMOST

The LAMOST project derived homogeneous spectroscopic parameters from low-resolution ($R \sim 1800$) LAMOST DR5 spectra for approximately 40% of the Kepler field (Zong et al. 2018; Xiang et al. 2019). The Xiang et al. (2019) catalog derived stellar parameters using the DD-Payne pipeline, which builds on the method of Ting et al. (2017) by incorporating elements of the Cannon (Ness et al. 2015) and uses the overlap with GALAH DR2 and APOGEE DR14 as training data. We cross-

matched the **LAMOST DR5** stellar parameter catalog of Xiang et al. (2019) with the McQuillan et al. (2014) catalog, which published rotation periods for >34000 Kepler targets, as well as the Santos et al. (2021) catalog, which provides rotation periods for >55000 FGKM stars observed by Kepler.

We matched 10844 LAMOST targets to 10550 unique Kepler IDs in the McQuillan et al. (2014), resulting in a sample with well-determined P_{rot} and spectroscopic T_{eff} (having a median error of 24 K). For the Kepler sources with duplicate cross-matched LAMOST sources we kept the source with a brighter Gaia DR2 G magnitude. In the Santos et al. (2021) sample we found 54982 unique cross-matched sources in LAMOST, of which 18990 have published temperatures and rotation periods. The metallicity distribution of the LAMOST–McQuillan sample is centered near solar, with a mean and standard deviation of -0.1 dex and 0.26 dex, respectively. There is negligible overlap (3 stars) between our LAMOST–McQuillan sample and the CKS sample since the McQuillan et al. (2014) did not publish rotation periods for KOIs, which were the targets of the CKS project. Rotation periods for KOIs are instead published in McQuillan et al. (2013b), as discussed in §2.1. Visualizations of the LAMOST–McQuillan and LAMOST–Santos samples are shown in Figure 2.

2.3. APOGEE

The Apache Point Observatory Galactic Evolution Experiment (APOGEE; Majewski et al. 2017) is a large-scale, high-resolution ($R \sim 22500$) stellar spectroscopic survey conducted at H -band as part of the Sloan Digital Sky Survey (SDSS-IV; Blanton et al. 2017). The

² <http://10.0.20.161/zenodo.4645437>

spectroscopic analysis pipeline for SDSS DR16 is described in Jönsson et al. (2020). We used Gaia DR2 source IDs (Gaia Collaboration et al. 2016, 2018) to cross-match Megan Bedell’s Gaia–Kepler catalog³ with the APOGEE DR16 catalog (Ahumada et al. 2020). Kepler IDs were then used to cross-match this table with the McQuillan et al. (2014) catalog. While the current overlap between Kepler targets and APOGEE is small compared to the LAMOST catalog, APOGEE DR17 will contain more dwarf stars and provide a better resource for studies such as ours. The focus of this work are overdensities in the $T_{\text{eff}} - P_{\text{rot}}$ plane, and as these appear to be less prominent when using APOGEE DR16 temperatures (Figure 1) we conclude that LAMOST and CKS provide more precise estimates of T_{eff} and do not analyze the APOGEE sample further.

2.4. The Sun

To place the Sun in the context of the long-period pile-up, we use up-to-date estimates of the Sun’s effective temperature, rotation period, and age. Following the IAU 2015 Resolution B3 (Prša et al. 2016), we take the nominal effective temperature of the Sun to be $T_{\text{eff},\odot}^N = 5772 K. For the solar rotation period we adopt the equatorial rotation period of $P_{\text{eq},\odot} \approx 25$ d with an upper error that encompasses the period of ≈ 36 d measured near the poles from differential rotation studies (Thompson et al. 2003, and references therein). The age of the Sun is assumed to be 4.567 Gyr from Pb-Pb dating of calcium-aluminum inclusions and chondrules recovered from primitive meteorites (Bahcall et al. 1995, and references therein).$

3. ANALYSIS

3.1. Initial observations

We first noted a pile-up of stars along the long-period edge for stars with $T_{\text{eff}} > 5800$ K when examining the $T_{\text{eff}} - P_{\text{rot}}$ plane for the CKS sample, using the CKS T_{eff} values and the vetted rotation period compilation from David et al. (2021). Sourcing rotation periods from McQuillan et al. (2013b); Mazeh et al. (2015) and Angus et al. (2018) revealed that this pile-up is still apparent when adopting periods uniformly from a single catalog (Figure 15). A secondary pile-up at the short-period edge is also apparent, though less pronounced, in the $T_{\text{eff}} - P_{\text{rot}}$ distribution of the LAMOST–McQuillan sample. We verified through inspection that the secondary pile-up does not lie along the $P_{\text{rot}}/2$ harmonic line of the long-period pile-up. As shown in Figure 3, This

secondary pile-up is seen most clearly through applying Gaussian kernel density estimation (KDE), which was performed with the `seaborn` package (Waskom et al. 2017).

The location of the **long**-period pile-up is close to the empirical hybrid cluster sequence derived by Curtis et al. (2020) from members of the NGC 6819 (age ~ 2.5 Gyr) and Ruprecht 147 (age ~ 2.7 Gyr) open clusters (Figure 3). Notably, we use the color– T_{eff} relation presented by those authors to recast the cluster sequences in terms of T_{eff} . As we show in §3.5, stars along the pile-up have a range of ages. Therefore, the observation that the edge approximately corresponds with the ~ 2.5 – 2.7 Gyr cluster sequence implies that stars with $T_{\text{eff}} \gtrsim 5500$ K have already piled up onto the edge by or before this timescale. Similarly, the edge is well-separated from the empirical ~ 1 Gyr cluster sequence based on rotation rates in the NGC 6811 cluster (Curtis et al. 2019a, 2020), implying that it takes F-type stars > 1 Gyr to reach the long-period edge. These observations are in accordance with predictions from the WMB model which suggest the pile-up forms on a timescale of 2–3 Gyr (van Saders et al. 2019).

In both the CKS and LAMOST samples, there is a change of slope along the ridge, with an inflection point corresponding closely to the Kraft break at ≈ 6250 K, the point at which convective envelopes become vanishingly thin (Kraft 1967). A piecewise linear fit to the ridge in the CKS sample confirmed that the inflection point occurs at $T_{\text{eff}} = 6250 \pm 32$ K, where the uncertainty was estimated from Markov chain Monte Carlo (MCMC) sampling. This change in slope is likely due to the fact that the convective turnover timescale, τ_{cz} , changes rapidly above 6250 K.

In the CKS sample, there appears to be a clustering of stars above the ridge with $T_{\text{eff}} > 6100$ K (seen most clearly in the top panels of Figure 4). This cluster of points has a similar slope in the $T_{\text{eff}} - P_{\text{rot}}$ plane as the long-period pile-up, and does not reside on the harmonic of the ridge line as one might expect if the periods were erroneously determined. After inspecting the light curves of stars on the ridge and above the ridge in the temperature range $6100 \text{ K} < T_{\text{eff}} < 6300$ K we did not notice any obvious trends or differences between the two samples. The periods of the stars in the cluster above the ridge appear to be just as reliable as those on the ridge. Interestingly, a similar clustering of points is not observed in the **LAMOST–McQuillan** sample and is less pronounced or absent when substituting the CKS temperatures with T_{eff} from either Brewer & Fischer (2018) or Martinez et al. (2019), two studies that independently derived spectroscopic parameters from the

³ <https://gaia-kepler.fun/>

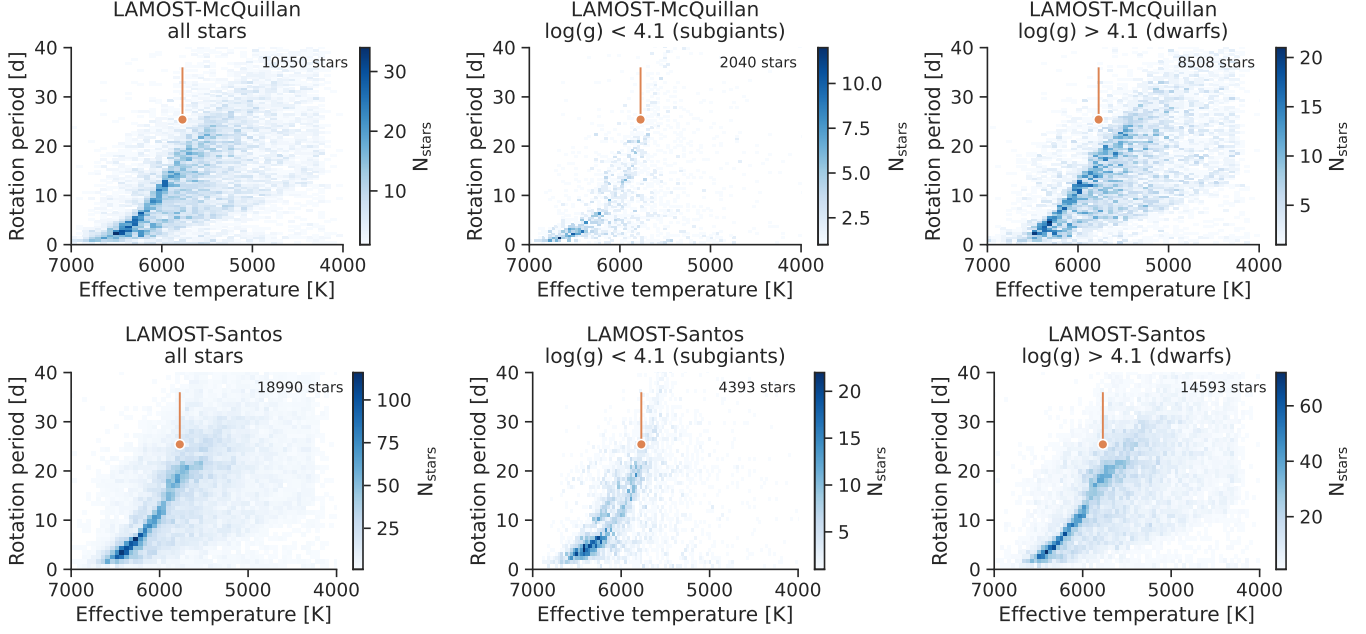


Figure 2. Two-dimensional histograms indicating the number of Kepler target stars in the T_{eff} – P_{rot} plane for the LAMOST–McQuillan sample (top row) and the LAMOST–Santos sample (bottom row). The effects of a simple cut in $\log g$ to separate subgiants and dwarfs are shown in the middle and right columns. In each panel the Sun is indicated by the orange point, with an errorbar reflecting the range of periods measured from its differentially rotating surface. The long-period pile-up for dwarf stars is clearly seen to extend to the solar temperature. The short-period pile-up is clearer in the smaller LAMOST–McQuillan dwarf sample, potentially because the Santos et al. (2021) catalog detected more stars at longer periods. The secondary overdensity observed in the subgiant samples, most visible in the bottom center panel, appears to be at twice the period of the primary overdensity, potentially due to erroneously determined rotation periods.

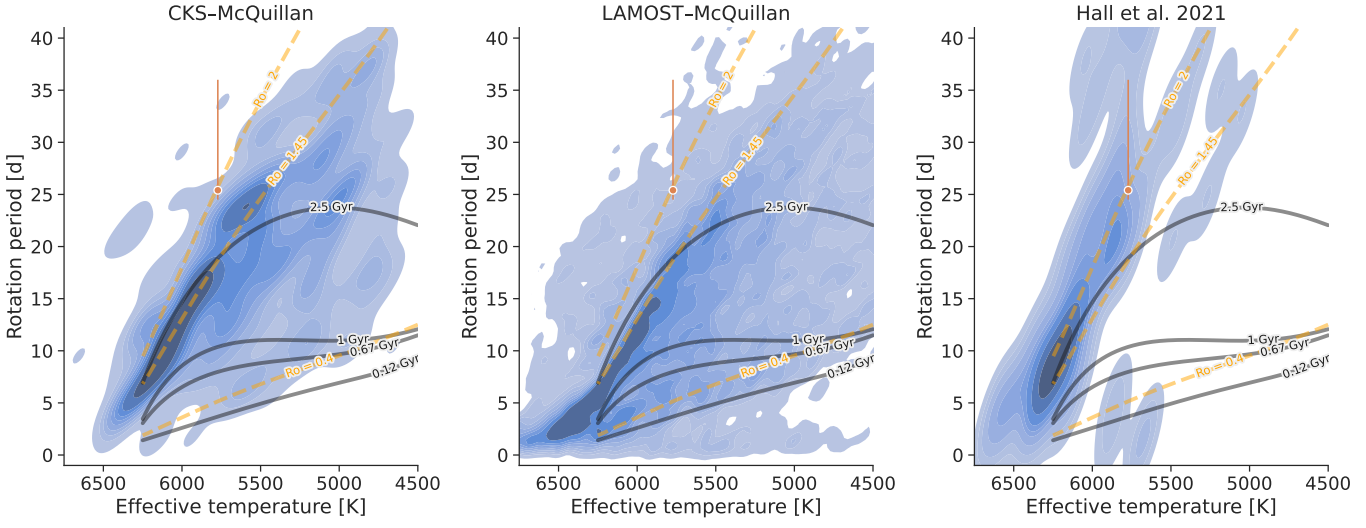


Figure 3. Gaussian kernel density estimation (blue contours) of the T_{eff} – P_{rot} distributions of the CKS–McQuillan, LAMOST–McQuillan, and asteroseismic Hall et al. (2021) samples, from left to right. Empirical cluster sequences from Curtis et al. (2020) are shown by the dark grey lines. The orange dashed lines show constant Rossby curves of fiducial values (see §3.4). The short-period pile-up can be observed in the LAMOST–McQuillan sample for $T_{\text{eff}} \gtrsim 5500$ K. The orange point indicates the Sun’s temperature and equatorial rotation period, with the errorbar capturing the range of periods measured from its differentially rotating surface.

CKS spectra. Further inspection of the stars in this cluster revealed that they have anomalously large T_{eff} discrepancies between the CKS and SPOCS catalogs, such that the SPOCS temperatures shift the stars onto the long-period pile-up. We conclude that the temperatures for these stars in the CKS catalog are too high by $\gtrsim 100$ K.

3.2. Comparison with theory

We compared the $T_{\text{eff}}-P_{\text{rot}}$ distribution of the CKS and **LAMOST–McQuillan** samples with the theoretical predictions of van Saders et al. (2019). Those authors presented forward modeling simulations of the observed Kepler P_{rot} distribution including theoretical models of stellar angular momentum evolution (for both the standard spin-down and WMB scenarios), a galactic population model, and a prescribed observational selection function. The theoretically predicted $T_{\text{eff}}-P_{\text{rot}}$ distributions of van Saders et al. (2019) are shown in relation to the observations in Figure 4. Neither model satisfactorily matches the observations, though the WMB model more closely matches the long-period edge of F-type and early G-type stars. The specific WMB prescription of van Saders et al. (2019) adopted a critical Rossby number of $\text{Ro}_{\text{crit}} = 2.08$, leading to a pile-up that is located at larger P_{rot} values (at fixed T_{eff}) when compared to the observations. Figure 5 shows the same models in relation to the data with constant T_{eff} offsets applied to the data, which are derived in §3.4. The T_{eff} offsets lead to better agreement between the data and models, although the long-period pile-up in the LAMOST–McQuillan sample appears to overlay the models only for $T_{\text{eff}} \gtrsim 6000$ K, possibly due to strong systematics in the LAMOST T_{eff} scale (see Appendix B).

To quantify the degree of agreement between the theoretical models and observations we computed the 10th and 90th percentile P_{rot} ranges of the standard and WMB models in overlapping T_{eff} bins, analogous to how the upper and lower boundaries of the observed P_{rot} distribution were found in §3.4. We computed the χ^2 values between the observed upper edge and the 90th percentile ranges of the standard and WMB models, finding the WMB model is preferred with a $\Delta\chi^2 = 154$. Moreover, the WMB model better reproduces the slope of the observed long-period edge between 5300–6000 K (Figure 6).

While better agreement between the WMB model and observations might be achieved with stalling at a lower Ro_{crit} , it is also possible that there are systematic offsets in the T_{eff} scales between the observations and models used in van Saders et al. (2019), as well as differences in the computation of τ_{cz} . We also note that, while the

models were computed using a simulated Kepler stellar population and selection function, the actual observed population and selection function of the **LAMOST–McQuillan** may be slightly different.

Shifting the LAMOST T_{eff} to higher values would bring the data into better agreement with the models. In turn, it appears that the long-period edge for lower mass stars would be at higher P_{rot} than the models (i.e. the low-mass stars would be rotating more slowly than the model predictions). Such a discrepancy could result from different underlying populations between the models and the LAMOST–McQuillan sample, or a different normalization for the magnetic braking law. The models above employ a modified magnetic braking law that is scaled to match the rotation period of the Sun (see equations 1 & 2 of van Saders & Pinsonneault 2013), with a normalization factor of $f_K = 6.6$. A higher normalization factor would cause the low-mass stars to spin down more at fixed age.

Notably, both models fail to reproduce the observed short-period pile-up, possibly due to the assumption of solid-body rotation in both models. At early times, Sun-like and low-mass stars are expected to have strong radial differential rotation due to their rapid collapse onto the main-sequence. The core and envelope at these times are thus assumed to be decoupled. However, the core and envelope are expected to couple on timescales of a few tens of million years for Sun-like stars (Denissenkov et al. 2010; Gallet & Bouvier 2015; Lanzaflame & Spada 2015) or hundreds of million years for low-mass stars (Gallet & Bouvier 2015; Lanzaflame & Spada 2015; Somers & Pinsonneault 2016). When this happens, angular momentum can be transferred from the core to the envelope at a rate comparable to the rate at which angular momentum is lost via magnetized winds. Consequently, so-called “two-zone” models (MacGregor & Brenner 1991) spin more rapidly than solid-body rotators at the same age. This hypothesis is discussed further in §4.2.

3.3. Comparison with asteroseismic rotation rates

Hall et al. (2021) determined rotation periods for 91 main-sequence, asteroseismic Kepler targets from rotational splitting of asteroseismic oscillation frequencies. We found that the distribution of the asteroseismic sample in the $T_{\text{eff}}-P_{\text{rot}}$ plane approximately matches the pile-up we observe, although the Hall et al. (2021) sample appears shifted slightly to either higher P_{rot} or higher T_{eff} values relative to the ridge in the **LAMOST–McQuillan** sample while such an offset is either absent or not as apparent relative to the CKS sample. Such an offset could be due to differing spectroscopic tem-

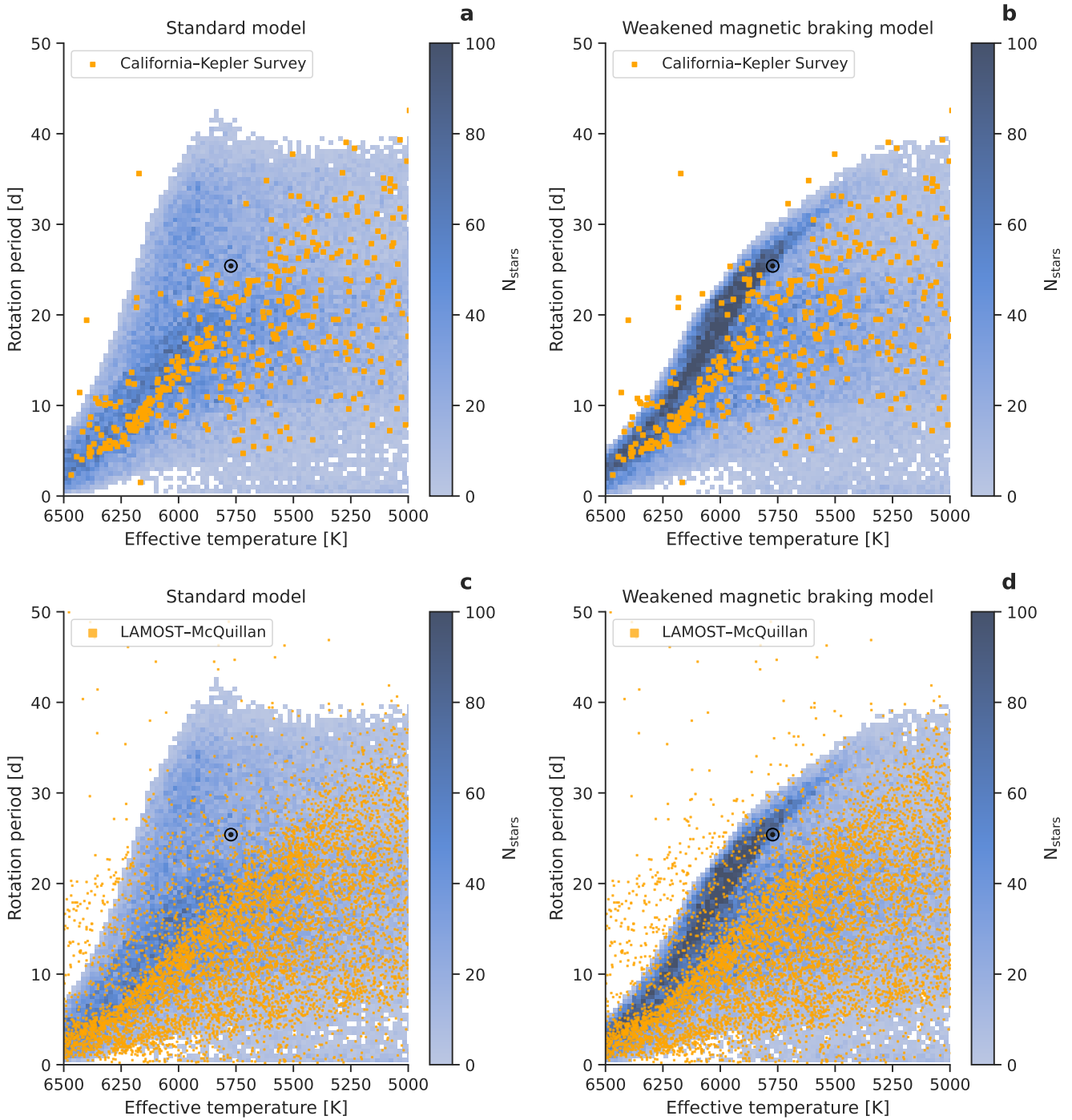


Figure 4. The $T_{\text{eff}}-P_{\text{rot}}$ plane for the CKS sample (top panels) and LAMOST sample (bottom panels) in comparison to the standard and WMB models (2-d histograms) presented in van Saders et al. (2019). Shown here are stars with $\log g > 4.1$. Rotation periods for the CKS sample here are sourced from the David et al. (2021) compilation. The black symbol in each panel indicates the position of the Sun.



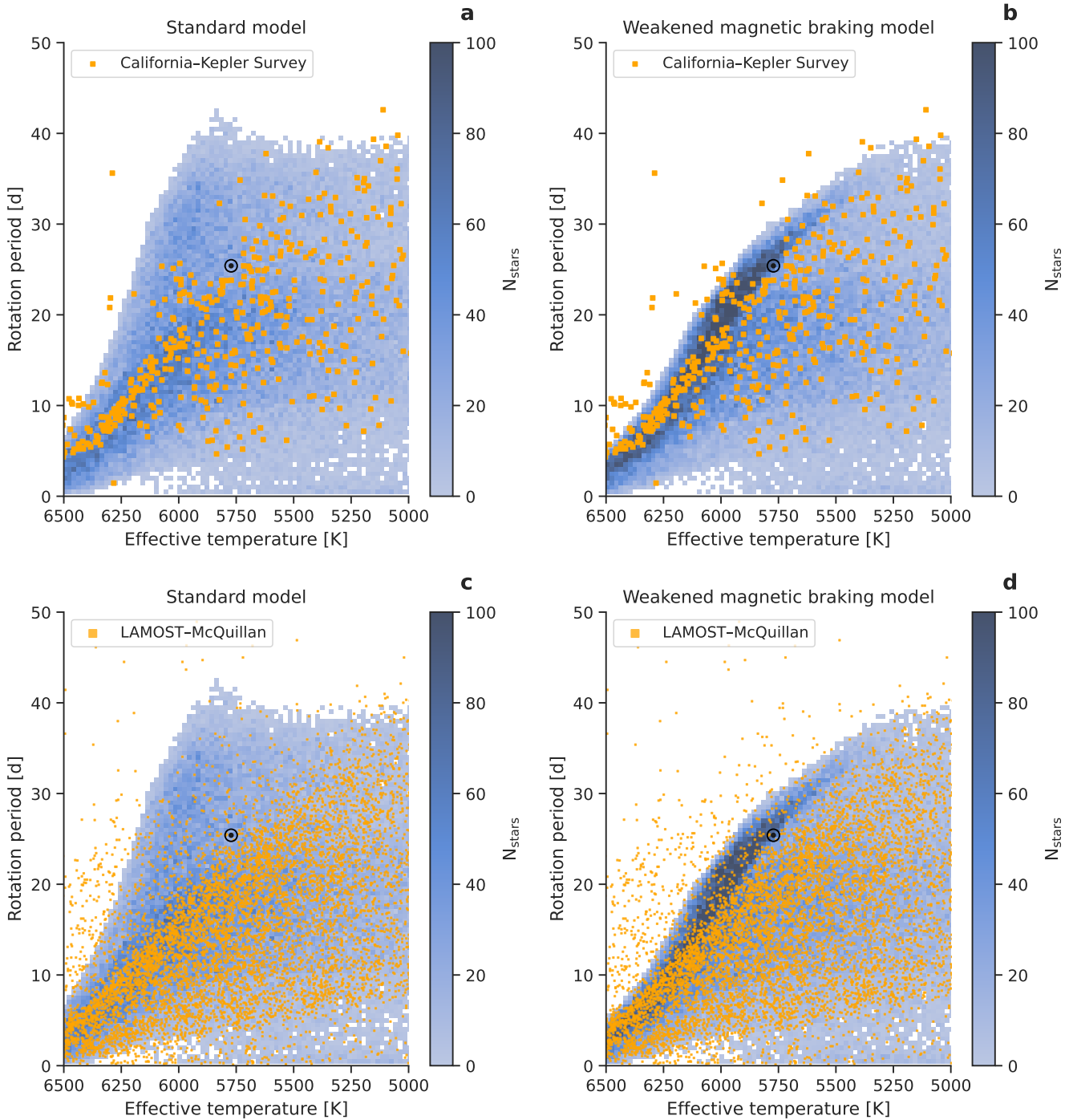


Figure 5. Same as Figure 4 with constant T_{eff} offsets applied to the data. Shifts of +116 K and +140 K are applied to the CKS and LAMOST T_{eff} , respectively. The CKS T_{eff} shift originates from a least-squares fit of a $\text{Ro}_{\text{crit}} = 2$ curve (with a T_{eff} offset) to the long-period pile-up (as described in §3.4). The LAMOST shift is derived in a similar fashion, with an additional +34 K offset which represents the systematic offset between CKS and LAMOST (see Appendix B).



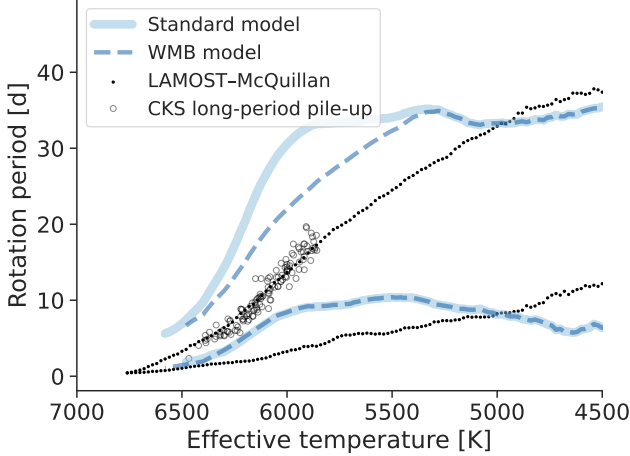


Figure 6. Discrepancies between the observed and theoretically predicted $T_{\text{eff}} - P_{\text{rot}}$ distribution of Kepler stars. Comparison of the 10th and 90th P_{rot} percentiles predicted from the standard (light blue) and WMB (blue) models of van Saders et al. (2019) with the same percentile ranges from the LAMOST–McQuillan sample (black points).

perature scales between the two studies. To investigate the origin of this offset, we cross-matched the Hall et al. (2021) sample with the LAMOST DR5 catalog (Xiang et al. 2019). We found a root mean square (RMS) of the residuals between the Hall et al. (2021) and LAMOST T_{eff} measurements of 55 K, with a median offset of 41 K, such that the LAMOST T_{eff} scale is cooler, on average. Though this discrepancy is modest, adopting the LAMOST T_{eff} scale appeared to resolve most of the offset between the pile-up as seen in the two samples.

3.4. Constant Rossby model

In the WMB model of van Saders et al. (2016, 2019), a star spins down until it reaches a critical Rossby number, at which point magnetic braking ceases. Since Rossby number is highly sensitive to temperature through its dependence on the convective turnover timescale ($\text{Ro} = P_{\text{rot}}/\tau_{\text{cz}}$, where τ_{cz} is the convective turnover timescale), this critical threshold corresponds to different rotation periods for stars of different T_{eff} , leading to a pile-up in the $T_{\text{eff}} - P_{\text{rot}}$ plane. Using a small sample of Kepler targets with rotation periods determined from brightness modulations, van Saders et al. (2016) proposed this threshold happens at a critical Rossby number of $\text{Ro}_{\text{crit}} \sim \text{Ro}_{\odot}$.

We tested the hypothesis that the long-period pile-up observed in the LAMOST–McQuillan sample is due to WMB by fitting constant Rossby models to the P_{rot} boundary. For a given T_{eff} , this model predicts P_{rot} as:

$$P_{\text{rot}}(\text{Ro}, T_{\text{eff}}) = \text{Ro} \times \tau_{\text{cz}}(T_{\text{eff}}), \quad (1)$$

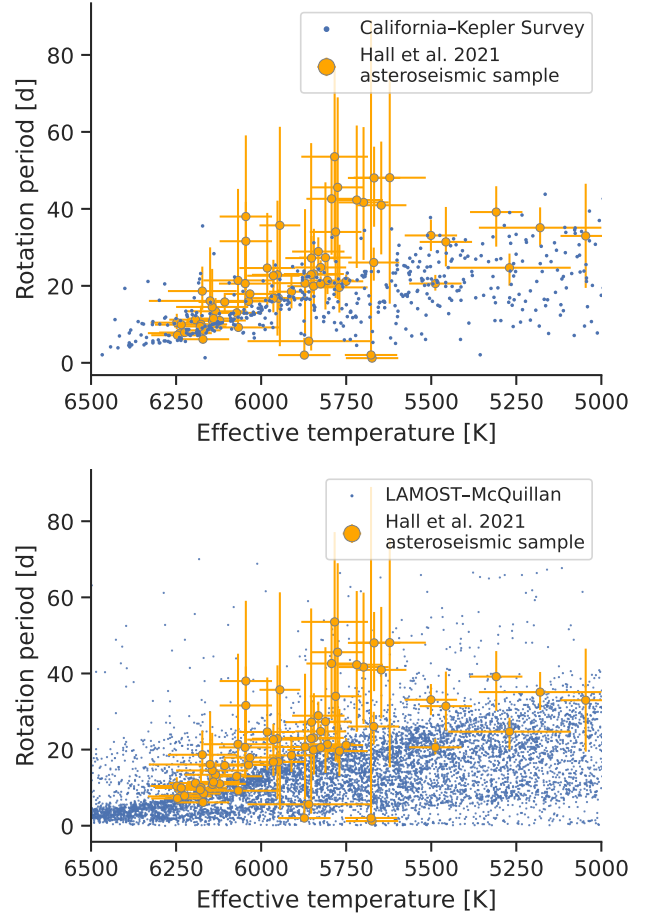


Figure 7. Comparison of CKS (left) and LAMOST–McQuillan samples (right) with the Hall et al. (2021) main-sequence asteroseismic sample in the $T_{\text{eff}} - P_{\text{rot}}$ plane. Note, the CKS, LAMOST, and Hall et al. (2021) samples derive T_{eff} from distinct pipelines. A constant offset of +41 K was applied to the LAMOST T_{eff} to bring that sample onto the same scale as the asteroseismic sample (see Appendix B). Using LAMOST T_{eff} , where it exists, for the Hall et al. (2021) sample brings that sample into even closer agreement with the long-period pile-up in the LAMOST–McQuillan sample.

where we used the equation for the convective turnover timescale (valid in the T_{eff} range of $3300 \text{ K} \lesssim T_{\text{eff}} \lesssim 7000 \text{ K}$) presented in Gunn et al. (1998) and replicated in Cranmer & Saar (2011):

$$\tau_{\text{cz}}(T_{\text{eff}}) = 314.24 \exp \left[- \left(\frac{T_{\text{eff}}}{1952.5 \text{ K}} \right) - \left(\frac{T_{\text{eff}}}{6250 \text{ K}} \right)^{18} \right] + 0.002. \quad (2)$$

To obtain a reasonable description of the long-period edge we computed the 90th percentile of P_{rot} values in overlapping T_{eff} bins with centers located every 20 K between 4000 K and 7000 K and half-widths of 100 K. We

found it was also necessary to omit stars with $\text{Ro} > 5/3$ in this computation to match the long-period edge. Since we observed a break in the 90th percentile P_{rot} curve near $T_{\text{eff}} = 4250$ K, due to smaller sample sizes at low T_{eff} , we restricted the analysis below to stars with $T_{\text{eff}} > 4250$ K. To compute approximate uncertainties on the 90th percentile curve we performed 100 bootstrapped resamplings in each bin, leaving out 50% of the data for each resampling. The 90th percentile curve and its uncertainty was then computed from the mean and standard deviation of the bootstrapped values. We computed the 10th percentile curve and its uncertainty similarly, as an approximation to the lower boundary of the $T_{\text{eff}}\text{-}P_{\text{rot}}$ plane. We show these curves in relation to the full **LAMOST–McQuillan** sample and to constant Rossby models in Figure 8.

We performed an initial Levenberg-Marquardt non-linear least-squares fit of a constant Rossby model to the long-period edge with the `curve_fit` function in the `scipy.optimize` class to optimize the following likelihood:

$$\ln p(y|T_{\text{eff}}, \sigma, \text{Ro}, f) = -\frac{1}{2} \sum_n \left[\frac{(y_n - P_{\text{rot}}(\text{Ro}, T_{\text{eff}} - T_{\text{sys}}))^2}{s_n^2} + \ln(2\pi s_n^2) \right], \quad (3)$$

where

$$s_n^2 = \sigma^2 + f^2 P_{\text{rot}}(\text{Ro}, T_{\text{eff}} - T_{\text{sys}})^2, \quad (4)$$

and y_n is the value of a P_{rot} percentile curve in the n th T_{eff} bin. This is a Gaussian likelihood where the variance is underestimated by some fraction, f . Here T_{sys} is a constant to allow for a systematic offset between the data and the models used to calibrate the τ_{cz} relation. We performed Markov chain Monte Carlo sampling (MCMC) of this likelihood with the `emcee` package (Foreman-Mackey et al. 2013, 2019) to estimate the mean and uncertainty of the critical Rossby number that best matches the long-period edge in the range of 5000 K $\lesssim T_{\text{eff}} \lesssim$ 6250 K. We instantiated 32 walkers around the least-squares solution and sampled for 10^5 steps, adopting uniform priors on Ro , f , and T_{sys} with ranges of (0.1, 10), (0, 10), and (-1000 K, 1000 K), respectively. Convergence was assessed by ensuring the chain length was at least 100 times longer than the chain autocorrelation lengths for each parameter. A similar analysis was performed for the 10th percentile curve, restricted in the range of 4500 K $\lesssim T_{\text{eff}} \lesssim$ 5800 K where a constant Rossby model provides a reasonable fit.

We additionally fit the CKS long-period pile-up (using three different homogeneous T_{eff} sources) and the Hall et al. (2021) asteroseismic main-sequence sample, allowing for T_{eff} offsets in each data set (Table 1). For the CKS pile-up stars and the LAMOST–McQuillan percentile curves, we assumed constant fractional P_{rot} uncertainties of 10%. To isolate the long-period pile-up stars in the CKS sample, we selected a trapezoidal region using the condition $-0.0314 T_{\text{eff}} + 199.286 < P_{\text{rot}} < -0.0314 T_{\text{eff}} + 206.286$. We note that this selection is particular to the CKS T_{eff} scale and is not general. For the CKS sample, we additionally required $\log g > 4$ and $5850 \text{ K} < T_{\text{eff}} < 6500$ K.

The constant Rossby model provides a reasonably good description of the LAMOST–McQuillan long-period edge in the T_{eff} range of $\approx 5000\text{--}6250$ K, with fractional residuals $\lesssim 5\%$ over this range. Above and below this T_{eff} range we see clear and significant divergence from the constant Rossby model, such that the model under-predicts periods of hotter stars and over-predicts periods of cooler stars, possibly because the cooler stars have not had enough time to evolve to the critical Rossby number associated with weakened magnetic braking (see Figure 6 in van Saders et al. 2019).

We caution that the specific values of Ro_{crit} found here are highly sensitive to shifts in the T_{eff} scales between the models and observations, as well as the T_{eff} scale of the models used to derive the τ_{cz} relation. Therefore, while we find values of $\text{Ro}_{\text{crit}} \lesssim 2$ are able to explain the various individual data sets, a value of $\text{Ro}_{\text{crit}} \approx 2$ is compatible with all of the data sets if modest T_{eff} systematics are present. Comparison of the long-period pile-ups as seen in the CKS and LAMOST–McQuillan samples support the notion that the LAMOST T_{eff} scale is about 30–40 K cooler than the CKS scale (see also Appendix B).

To further explore whether our Ro_{crit} inference procedure is biased by systematics in the data, we performed non-linear least-squares fits of two models to the CKS long-period pile-up and the LAMOST–McQuillan 90th percentile curve (both in the T_{eff} range of 5800–6250 K) using the `curve_fit` function in `scipy.optimize`. The first model assumes $\text{Ro}_{\text{crit}} = 2$ and has one free parameter, a temperature shift added to the data. The second model assumes no temperature shift and allows Ro_{crit} to vary (Ro_{crit} being the only free parameter). The results of these fits are shown in Figure 9. We found that for the CKS sample, particularly when using the more precise temperatures from Fulton & Petigura (2018), that the $\Delta\chi^2$ between the $\text{Ro}_{\text{crit}} = 2$ and variable Ro_{crit} models was negligible. In other words, the $\text{Ro}_{\text{crit}} = 2$ model fits the data well with a T_{eff} shift of $\approx 80\text{--}150$ K de-

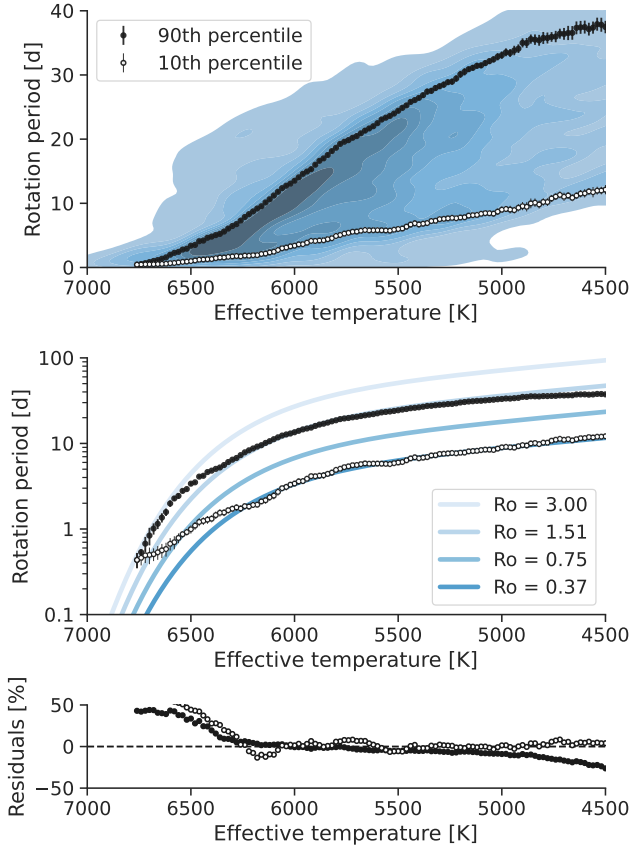


Figure 8. *Top:* Gaussian kernel density estimation of the LAMOST–McQuillan sample and the 10th and 90th P_{rot} percentiles (white and black points, respectively), computed as described in §3.4. *Middle:* The same 10th and 90th percentile curves shown in relation to constant Rossby curves. *Bottom:* Residuals from the median models resulting from the MCMC sampling. The fits depicted above do not include a T_{eff} offset.

pending on the T_{eff} source used. For the LAMOST–McQuillan sample, there is weak support for the variable Ro_{crit} model. However, as shown in Appendix B, there is a strong systematic trend in the LAMOST temperatures when compared to other spectroscopic catalogs (particularly SPOCS). Correcting for these systematic trends weakens the support for the variable Ro_{crit} model, and we speculate that temperature systematics bias the Ro_{crit} inference procedure. Lending further support to this hypothesis is the observation of visibly different slopes for the long-period pile-up in the CKS vs. LAMOST–McQuillan samples (see Fig. 6).

3.5. Ages of stars on the long-period pile-up

The WMB model predicts that hotter stars pile up on the long-period edge at younger ages, producing an age

gradient across the edge. In Figure 11 we show the T_{eff} –age distributions of stars on the ridge using ages from the CKS and SPOCS (Brewer & Fischer 2018) catalogs, where we use the trapezoidal selection described in §3.4 to select stars on the long-period pile-up. Both catalogs derive spectroscopic parameters from the CKS spectra, but use different pipelines for both the spectroscopic parameters and the isochrone fitting. In both cases, there appears to be an age gradient such that hotter stars are younger on average. However, such a trend is also expected in a sample of main-sequence stars as a natural consequence of the shorter main-sequence lifetimes of hotter, more massive stars. We also find that the dispersion in age is a sensitive function of T_{eff} , with cooler stars on the ridge showing a broader range of ages. This observation could be due to cooler stars populating the ridge for longer periods of time (relative to hotter stars), the lower precision of isochrone ages for cooler stars, or some combination of the two effects.

We determined that 90% of the stars on the ridge have ages between 1.4–5.6 Gyr (using ages from the CKS catalog), or 2.3–5.9 Gyr (using SPOCS ages). However, we note that systematic effects in surveys and theoretical models lead to large uncertainties in isochrone ages that are not necessarily represented by the reported age uncertainties. The SPOCS ages in particular are questionable given that only $\sim 1\%$ of the stars have ages < 2 Gyr and that stars are concentrated at the upper age boundary for a given T_{eff} (Figure 11). In fact, there are only a handful of long-period pile-up stars in the CKS sample with ages older than the age of the Sun (using CKS ages), and almost all of the pile-up stars would be compatible with an age equal to or less than the Sun’s given the large age uncertainties.

In the WMB model, although wind-driven angular momentum losses cease, stars continue to evolve structurally which results in evolution in the moment of inertia and stellar spin, driven by expansion of the stars away from the main-sequence (van Saders et al. 2019). Stars reach $\text{Ro}_{\text{crit}} \approx 2$ approximately halfway through their main-sequence lifetimes and remain there until the main-sequence turnoff. Thus, higher mass stars with shorter main-sequence lifetimes should show a smaller age spread on the long-period pile-up relative to lower mass stars with longer main-sequence lifetimes. Though we have not quantified such an age-gradient, the data suggest that some stars spend several Gyr occupying the ridge with only modest evolution of their spin rates.

We additionally selected stars on the long-period pile-up from the LAMOST–McQuillan sample by selecting stars with periods within 5% of the $\text{Ro} = 1.3$ curve (which traces the center of the highest den-

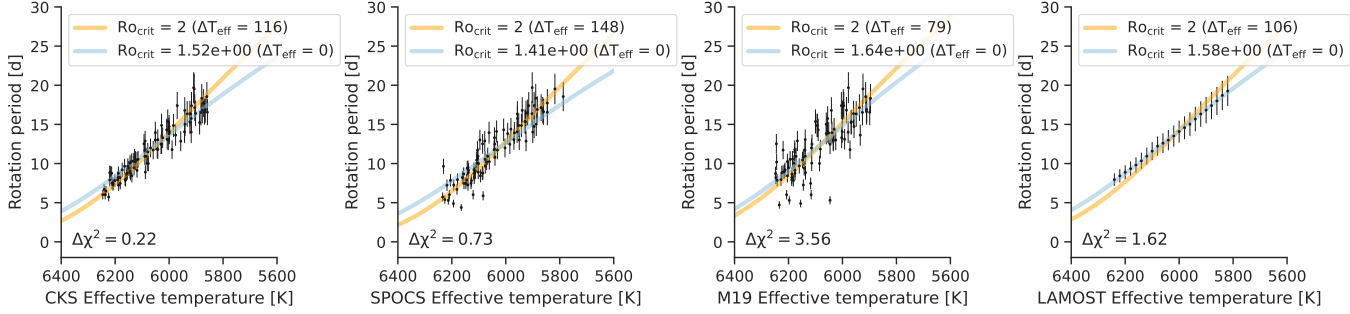


Figure 9. Non-linear least-squares fits to the long-period pile-up for a $\text{Ro}_{\text{crit}} = 2$ model with constant T_{eff} offset (orange) and a variable Ro_{crit} model with no T_{eff} offset (blue). The $\Delta\chi^2$ values printed in each panel are computed as $\chi^2_{\text{Ro}_{\text{crit}}=2} - \chi^2_{\Delta T_{\text{eff}}=0}$.

Table 1. Results of constant Rossby model fits.

Sample	T_{eff} range	Ro	f	T_{sys} (K)
<i>Short-period pile-up</i>				
LAMOST–McQuillan 10th P_{rot} pctl.	4500 K–5800 K	0.37 ± 0.02	0.011 ± 0.009	46 ± 80
<i>Long-period pile-up</i>				
LAMOST–McQuillan 90th P_{rot} pctl.	5000 K–6250 K	1.38 ± 0.04	0.011 ± 0.008	49 ± 19
LAMOST–McQuillan 90th P_{rot} pctl.	5800 K–6250 K	1.4 ± 0.1	0.019 ± 0.015	44 ± 43
CKS (CKS T_{eff})	5800 K–6250 K	1.77 ± 0.07	0.02 ± 0.01	-70 ± 15
CKS (SPOCS T_{eff})	5800 K–6250 K	1.9 ± 0.1	0.12 ± 0.01	-136 ± 23
CKS (M19 T_{eff})	5800 K–6250 K	1.6 ± 0.2	0.18 ± 0.02	21 ± 42
Hall et al. (2021) main-sequence	5000 K–6250 K	1.7 ± 0.2	0.30 ± 0.04	-5 ± 64
Hall et al. (2021) main-sequence	5800 K–6250 K	1.9 ± 0.4	0.27 ± 0.05	-29 ± 79

sity contour in Figure 3), $5500 \text{ K} < T_{\text{eff}} < 6500 \text{ K}$, and $4.1 \text{ dex} < \log g < 4.75 \text{ dex}$. While ages for the LAMOST–Kepler sample are not available, the broad distribution of these stars in the spectroscopic H-R diagram supports the inference from the CKS sample that the long-period pile-up is populated by stars with a broad range of ages (Figure 11). Interestingly, the solar T_{eff} and $\log g$ values appear to be wholly consistent with the distribution of long-period pile-up stars. We discuss the Sun in context of the long-period pile-up further in §4.4.

To further assess the evolutionary state of stars on the long-period pile-up, we constructed a color-magnitude diagram (CMD) from the Gaia DR2 photometry and parallaxes for the Kepler field, the McQuillan et al. (2014) and Santos et al. (2021) rotation period catalogs, the Hall et al. (2021) asteroseismic sample, and the CKS long-period pile-up stars from this work (Figure 10). As expected, the stars with detected periods from rotational brightness modulations are almost exclusively solar-type and lower-mass stars on the main-sequence. The Santos et al. (2021) catalog contains more stars, in part due to the higher sensitivity to more slowly rotating,

evolved stars, relative to McQuillan et al. (2014). CKS stars on the long-period pile-up clearly occupy a well-defined region of the main-sequence, which overlaps well with the Hall et al. (2021) asteroseismic sample.

3.6. Where do the pile-ups end?

It appears from Figures 3 and 4 that the number density of stars on the long-period pile-up declines towards cooler T_{eff} , as predicted by the WMB model (see Figure 13 of van Saders et al. 2019). The number density of stars on the short-period pile-up similarly declines towards cooler T_{eff} . If the short-period pile-up is due to core–envelope coupling, one might expect an opposite trend of increasing number density toward cooler T_{eff} , since the core–envelope coupling timescales and hence the “stalled” braking phases are longer for lower-mass stars (Curtis et al. 2020). However, the observed $T_{\text{eff}}–P_{\text{rot}}$ distribution will also depend sensitively on the selection functions and observational biases inherent to both Kepler and the source of T_{eff} (e.g. LAMOST). While it is not clear whether or not these declines are astrophysical in nature, the result of the selection functions or obser-

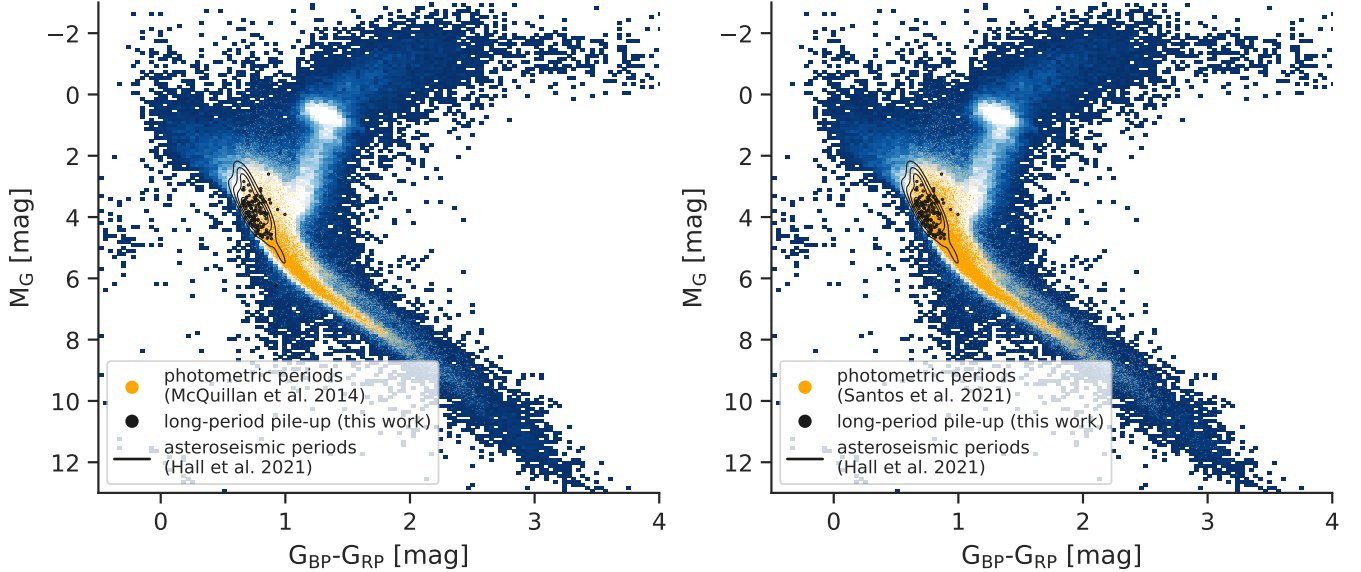


Figure 10. Color-magnitude diagram. The two panels are identical with exception of the orange points. In the background, a 2-d histogram of the Kepler field, where lighter shades represent a higher number of stars. Shown by orange points are stars with photometric rotation period detections from either the [McQuillan et al. \(2014\)](#) or [Santos et al. \(2021\)](#) catalogs, on the left and right, respectively. The CKS long-period pile-up stars identified in this work are shown by black points. A Gaussian kernel density estimation of the [Hall et al. \(2021\)](#) asteroseismic sample is shown by black contours.



vational biases inherent to Kepler or LAMOST, or some combination of effects, we attempted to characterize the extent of the pile-ups through the following approach. We found through inspection that constant Rossby curves of $\text{Ro}=0.5$ and $\text{Ro}=1.3$ (for the short- and long-period pile-ups, respectively) appear to describe the highest density contours found from Gaussian kernel density estimation of the LAMOST–McQuillan sample. In windows of 10 K width we measured the fraction of stars with periods within 1 d of each of the two constant Rossby curves, relative to the total number of stars in that T_{eff} window. We found that the relative fraction of stars on the long-period pile-up declines rapidly between 6500 K and 5800 K, by more than half in that temperature range before plateauing at cooler T_{eff} (Figure 12). The relative fraction of stars on the short-period pile-up declines more slowly, and below the temperature of the Sun, the relative fractions of stars on the two pile-ups are nearly equal. Thus, it is not yet clear if either pile-up extends to temperatures cooler than $T_{\text{eff},\odot}$.

4. DISCUSSION

4.1. Long-period behavior

As discussed in §3.2 and §3.4, the existence of a pile-up of stars with a constant Rossby number is consistent with expectations from the WMB model of [van Saders et al. \(2016, 2019\)](#). The location of the long-period pile-up coincides closely with the cluster of main-sequence stars with asteroseismic rotation rates determined by

[Hall et al. \(2021\)](#) and we suggest the two features are one and the same. Offsets in both observational and theoretical T_{eff} scales between different studies can explain the modest discrepancies between the asteroseismic sample and the samples considered here, as well as discrepancies in the Ro_{crit} values inferred here and those proposed in [van Saders et al. \(2019\)](#). Furthermore, we note that there are important differences between the samples considered here and the [Hall et al. \(2021\)](#) asteroseismic sample. The present samples have rotation periods detected from photometric variations and, for a survey of finite baseline and sensitivity like Kepler, photometric rotation periods are harder to detect for slower rotators, smaller amplitude variations, and more stochastic variability patterns. Exacerbating the problem of detection, slower rotation tends to be accompanied by smaller-scale and less periodic variability. The asteroseismic sample, by comparison, is not biased against quiet, unspotted stars and is more likely to contain pile-up stars that our sample may have missed. It is evident from Figure 13 that the long-period pile-up also coincides with a steep gradient in variability amplitude, such that a hidden population of pile-up stars may lie just beyond the edge of detectability. This effect, in addition to the T_{eff} offsets mentioned above, can further bias our inference of Ro_{crit} to lower values. Regardless of the biases mentioned above and the true value of Ro_{crit} , the sample considered clearly indicates that the long-period pile-up is apparent for stars with $T_{\text{eff}} \gtrsim 5500$ K

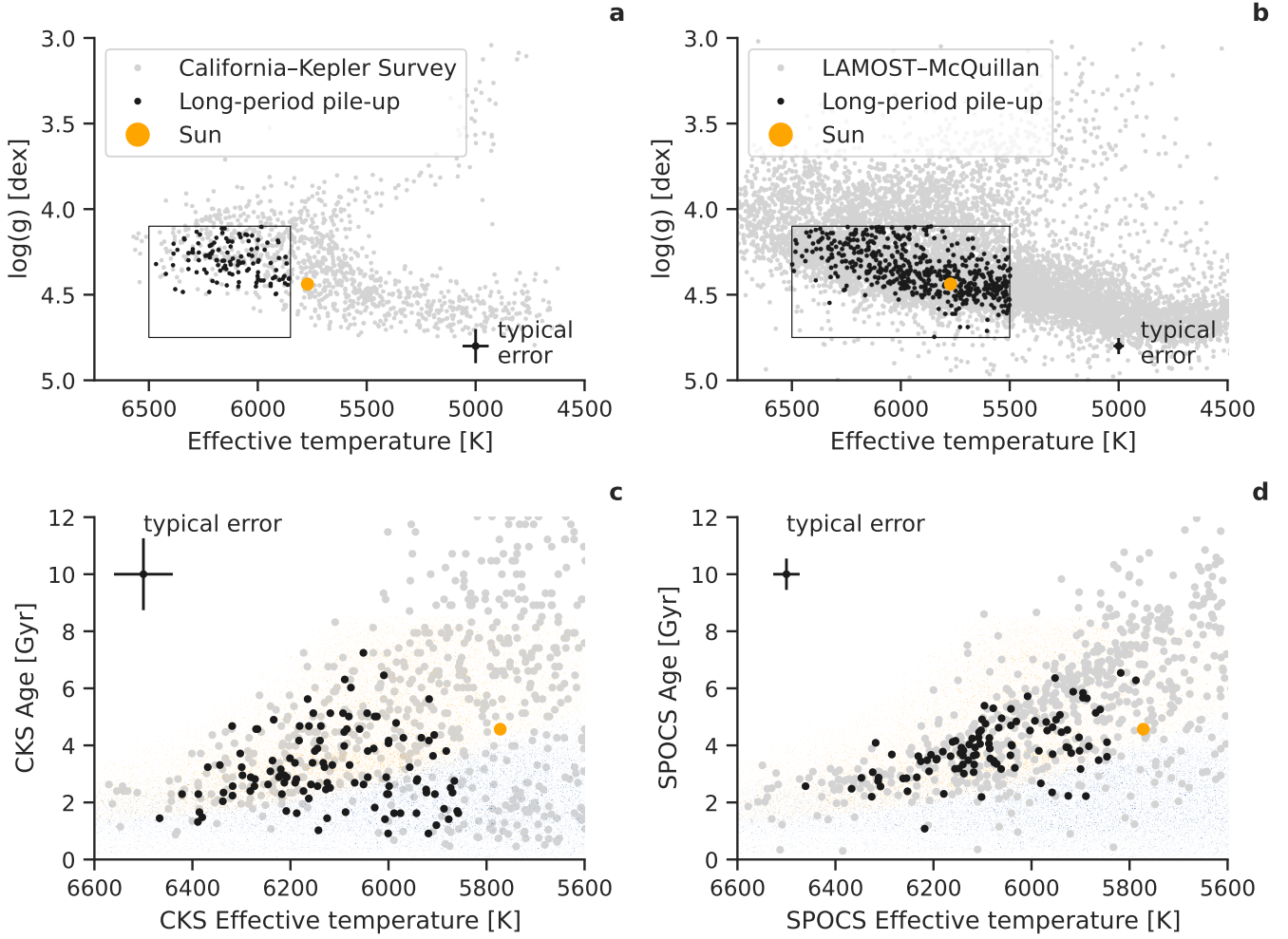


Figure 11. Above, H-R diagram placement of long-period pile-up stars relative to the Sun and the CKS sample (a) and similarly for the LAMOST–McQuillan sample (b). Below, the T_{eff} -age plane for CKS stars along the long-period pile-up using isochrone ages from the CKS (c) and SPOCS (d) catalogs. The light shaded points represent predictions from the WMB model of van Saders et al. (2019) for stars with $\text{Ro} < 2$ (blue) and $\text{Ro} > 2$ (orange). Note, panels (a), (c), and (d) all pertain to the CKS sample, whereas panel (b) relates to the LAMOST–McQuillan sample, for which homogeneous ages have not been published.



with Rossby numbers lower than those associated with a detection edge.

Recently, Lorenzo-Oliveira et al. (2019) studied the P_{rot} –age relation of solar twins observed by the Kepler mission, finding marginal statistical evidence in favor of a standard spin-down model over the WMB model. Those authors posited that if WMB takes place for Sun-like stars, it should happen at $\text{Ro}_{\text{crit}} \gtrsim 2.29$ or ages $\gtrsim 5.3$ Gyr.⁴ By comparison, our findings provide support for the WMB model among stars that are slightly hotter than the Sun, but at $\text{Ro}_{\text{crit}} \lesssim 2$ and at ages in the range of ~ 2 – 6 Gyr. In contrast to the find-

ings of those authors, we find that the long-period pile-up lies clearly below an empirical 2.5 Gyr gyrochrone of Curtis et al. (2020) that is evolved forward to 5.3 Gyr for braking indices of $n = 0.5$ or $n = 0.65$.

We note that the Ro_{crit} values we found in §3.4 are smaller than the values of ~ 2 found by van Saders et al. (2016, 2019), however, these results are sensitive to different T_{eff} scales and different prescriptions for τ_{cz} . We explored the τ_{cz} formulae of Barnes & Kim (2010) and Landin et al. (2010), but these produce larger τ_{cz} at fixed T_{eff} than the Gunn et al. (1998) relation, which exacerbates the Ro_{crit} mismatch mentioned above.

4.2. Short-period behavior

Unlike the long-period pile-up, the short-period pile-up is not predicted by the WMB model or, more gen-

⁴ A case study of an ~ 8 Gyr solar twin further reinforced these conclusions (Lorenzo-Oliveira et al. 2020).

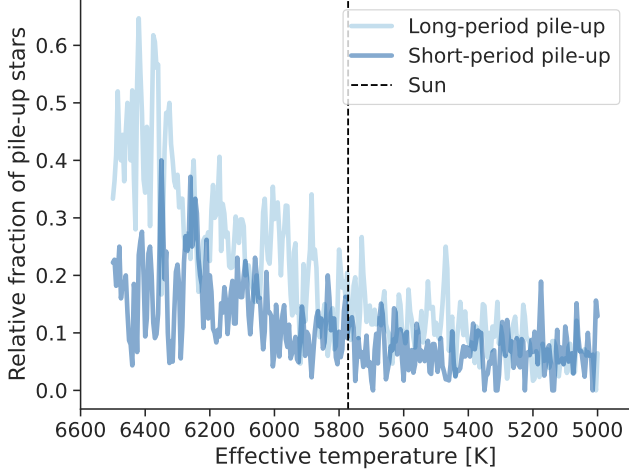


Figure 12. The relative fraction of stars on the long- and short-period pile-ups, in the LAMOST–McQuillan sample, in 10 K windows of T_{eff} (for stars with $\log g > 4.1$ dex).

erally, any standard, solid-body braking model. However, this feature may also be due to an epoch of apparent stalling, albeit a temporary one since cluster studies demonstrate that stars continue to spin down beyond the short-period pile-up. Works examining the $T_{\text{eff}} - P_{\text{rot}}$ sequences of open clusters have found overlap between low-mass members in clusters of different ages (Agüeros et al. 2018; Curtis et al. 2019a, 2020), notably Praesepe (0.67 Gyr), NGC 6811 (1.4 Gyr), and NGC 752 (1.4 Gyr). In other words, the spin rates of low-mass stars appear to evolve very little in the time elapsed between the ages of those clusters. The short-period pile-up we observe may be the manifestation of the same type of slowed spin evolution, but for stars of higher masses and younger ages than the cluster members in the above-mentioned works (since the pile-up is observed at shorter periods relative to the Praesepe sequence).

Curtis et al. (2019a, 2020) proposed that the overlapping cluster sequences could be produced by a temporary epoch of stalled spin-down, caused either by (i) a reduction in the magnetic braking torque, or (ii) core–envelope momentum transfer which offsets the effect of magnetic braking (e.g. MacGregor & Brenner 1991). In the core–envelope momentum transfer scenario angular momentum is exchanged between the envelope and the core on a characteristic timescale known as the core–envelope coupling timescale. The angular momentum transfer spins up the envelope, temporarily offsetting the spin-down via magnetic braking. Thus, in the core–envelope coupling scenario, spin evolution is slowed when the star’s age becomes comparable to the core–envelope coupling timescale. Theoretical predictions for the core–envelope coupling timescale for a

solar-mass star range from 30–110 Myr (MacGregor & Brenner 1991; Krishnamurthi et al. 1997; Bouvier 2008; Irwin & Bouvier 2009; Denissenkov et al. 2010; Gallet & Bouvier 2015; Lanzafame & Spada 2015; Somers & Pinsonneault 2016; Spada & Lanzafame 2020).

After a period of slowed spin-evolution, stars must resume spinning down as evidenced from studies of older open clusters. From open cluster data Curtis et al. (2020) estimated that solar-mass stars resume spin-down after an age of ≈ 230 Myr. Thus, if core–envelope coupling is responsible for delaying the spin-down of stars, and if the theoretical core–envelope coupling timescales are accurate, then we may expect Sun-like stars to experience slowed spin evolution between ~ 100 Myr and ~ 200 Myr.

Both the theoretically predicted core–envelope coupling timescale and the observationally inferred timescale for the resumption of spin-down are consistent with our observation that the short-period pile-up is intermediate to the Pleiades (0.12 Gyr) and Praesepe (0.67 Gyr) cluster sequences. Furthermore, in order to match observations of rotation periods in young clusters, models require that the core–envelope coupling timescale increases towards lower stellar masses (e.g. Irwin et al. 2007; Denissenkov et al. 2010; Gallet & Bouvier 2015), which provides a natural explanation for why this stalling occurs at older ages for lower-mass stars (Curtis et al. 2020).

We emphasize that the temporary epoch of slowed spin-down (also referred to as stalled magnetic braking) proposed by Curtis et al. (2019a, 2020) is not to be confused with the termination of magnetic braking that characterizes the WMB model of van Saders et al. (2016, 2019). The physical mechanisms thought to be responsible for each of these proposed stages of rotational evolution are distinct, though it is interesting that both the long- and short-period pileups seem to be well-described by curves of constant Rossby number. As mentioned above, one theory for the earlier stage of stalled spin-down is core–envelope coupling. Crucially, in the stalled spin-down phase, wind-driven angular momentum losses are not ceased but rather offset by the spin-up torque from core–envelope coupling. In contrast, in the WMB scenario, wind-driven angular momentum losses are proposed to cease ($dJ/dt=0$), with subsequent rotational evolution dictated by the changes in the moment of inertia.

4.3. Implications for the period gap

An unexplained feature of the Kepler rotation period distribution is the existence of a bimodal period distribution for dwarf stars of similar T_{eff} . The effect was first

noticed for M-dwarfs (McQuillan et al. 2013a), but was later shown to extend to ~ 5000 K (Reinhold et al. 2013; McQuillan et al. 2014; Reinhold & Hekker 2020), and even to ~ 6500 K (Davenport 2017).

McQuillan et al. (2013a, 2014) speculated that this period bimodality could originate from stellar populations of different ages, an explanation seemingly supported by a correlation between the strength of the bimodality and height above the galactic disk (Davenport & Covey 2018). However, Curtis et al. (2020) demonstrated that cluster sequences cross the gap, invalidating the claim that the feature is caused at a specific age, as one might expect from a period of decreased star formation. Additionally, Gordon et al. (2021) found that the gap is observed across the many fields observed by the K2 mission, which is in tension with the star formation history hypothesis as different Galactic sight lines are expected to have different different star formation histories (for sufficiently large volumes).

An alternative explanation for the gap was proposed by Reinhold et al. (2019), who found that the dearth of stars with intermediate rotation periods is associated with a decrease in photometric variability. Consequently, those authors proposed that the period bimodality may be the result of a transition between spot- and faculae-dominated photospheres. In this scenario, the period gap is due to bright faculae canceling out the effects of dark star spots.

The short- and long-period pile-ups we examine here naturally produce a dearth of rotators at intermediate periods. This gap is the same period gap noticed by the authors mentioned above, as made apparent when comparing the LAMOST–McQuillan sample to the original McQuillan et al. (2014) sample. Moreover, as seen in Figure 13, we recover the gradient in photometric variability across the gap pointed out by Reinhold et al. (2019). The photometric variability, as measured through the R_{per} metric published by McQuillan et al. (2014), reaches a local minimum near the location of the gap. This supports the notion that the cause of the gap is due to changes in the stars themselves, rather than being the result of mixed stellar populations. However, the variability levels on both sides of the gap are not close to the detection limit, as evidenced by the fact that periods are securely detected for stars with similar properties at much lower R_{per} values. This would suggest that the period gap is not due solely to a detection issue, unless variability levels were to drop precipitously as stars approached the gap. Gordon et al. (2021) proposed that the gap could instead be due to a period of accelerated spin-down immediately proceeding the stalling due to core–envelope coupling (such that

stars evolve quickly through the gap and are rarely observed there). We can neither confirm nor reject this scenario, and we note that the gap is significantly emptier when using Gaia colors (Davenport & Covey 2018; Gordon et al. 2021) compared to when using spectroscopic T_{eff} as we do here. Notably, if the short-period pile-up is indeed due to core–envelope coupling, and the gap due to a period of accelerated spin-down after such a coupling episode, the observed gradient in photometric variability still requires a physical explanation.

4.4. Does the Sun reside on the long-period pileup?

It is unclear whether or not the Sun is a resident of the long-period pile-up. From Fig. 2 it is clear that the long-period pile-up extends to temperatures as cool as the Sun’s. However, it is not clear whether there is a large systematic offset in the LAMOST temperature scale and the temperature scale of the Sun. If one assumes there are no systematic offsets between the two T_{eff} scales, the Sun’s equatorial rotation period places it $\sim 5\text{--}7$ days above the long-period pile-up. This raises the question of how the Sun’s angular momentum has evolved to its current state, and whether WMB is a generic evolutionary phase.

We consider the most likely explanation for the observed gap between the Sun and the long-period pile-up to be systematic offsets in T_{eff} . To place the Sun on the long-period pile-up would require shifting the spectroscopic temperatures higher by $\sim 50\text{--}100$ K for the CKS sample, $\sim 100\text{--}200$ K for the SPOCS sample, or $\sim 200\text{--}300$ K for the LAMOST sample. Notably, comparing the Sun to the Hall et al. (2021) asteroseismic sample (Figure 3) seems to support the notion that the Sun may indeed reside on the long-period pile-up, or very close to it, without the need for a T_{eff} shift. Furthermore, as discussed in §4.1, the Hall et al. (2021) sample is less prone to detection bias which acts to censor stars with higher Ro and lower variability amplitudes in the samples considered here. As shown by Aigrain et al. (2015), the pipelines used to measure rotation periods from Kepler data would not be guaranteed to detect the solar rotation period. We conclude that the Sun likely does reside on the long-period pile-up, but that this is obfuscated in the present samples by temperature offsets as well as potentially detection biases.

5. CONCLUSIONS

Our primary conclusions are summarized as follows:

1. We observe an overdensity at the long-period edge of the $T_{\text{eff}}\text{-}P_{\text{rot}}$ distribution of Kepler main-sequence stars with $T_{\text{eff}} \gtrsim 5500$ K. We hypothesize that this pile-up was previously obfuscated

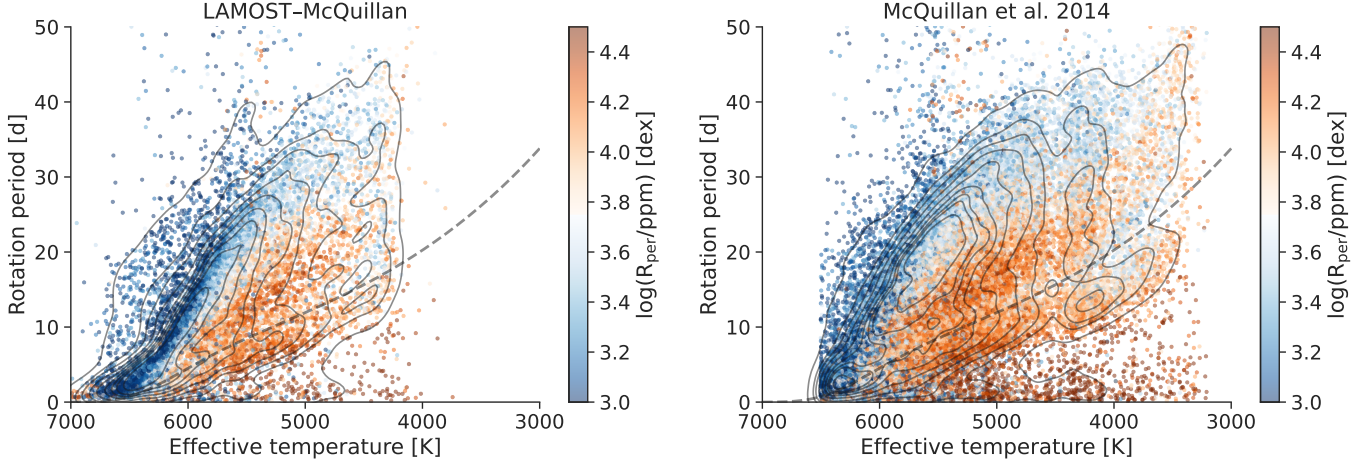


Figure 13. The $T_{\text{eff}} - P_{\text{rot}}$ distribution of the LAMOST–McQuillan (left) and McQuillan et al. (2014) samples color coded by the variability amplitude, R_{per} . Black contours show Gaussian kernel density estimation of the plotted distributions, and the dashed line shows a constant Rossby curve of $\text{Ro} = 0.5$. The long- and short-period pile-ups are separated by a relative dearth of stars with intermediate rotation periods. A strong gradient in R_{per} is apparent across this gap, such that variability amplitude reaches a local minimum near the gap’s center.

by imprecise T_{eff} estimates. Both the existence of the pile-up and its obscuration by large T_{eff} errors were predicted by van Saders et al. (2019) as a consequence of weakened magnetic braking for stars with $M \gtrsim 1 M_{\odot}$.

2. The long-period pile-up is well-described by a constant Rossby number, with a critical value of $\text{Ro}_{\text{crit}} \lesssim 2$, in the T_{eff} range of $\approx 5000\text{--}6250$ K. The pile-up is also populated by stars with a wide range of isochrone ages ($\sim 2\text{--}6$ Gyr). A pile-up of stars with a constant Rossby number and a broad range of ages is a prediction of the WMB model of van Saders et al. (2016, 2019). The precise value of Ro_{crit} is sensitive to T_{eff} scale shifts between observational data and the models used to compute τ_{cz} .
3. Comparison of the feature with empirical rotation sequences from open clusters implies that stars with $M \gtrsim 1 M_{\odot}$ pile up onto the ridge on a timescale > 1 Gyr but $\lesssim 2.5$ Gyr, compatible with the predictions of van Saders et al. (2019). Using isochrone ages for a sample of exoplanet hosts on the long-period pileup suggests that stars slightly hotter than the Sun may populate the pile-up until an age of ~ 6 Gyr.
4. It is yet unclear whether the Sun resides on the long-period pile-up or has already evolved through it. Shifts of $\sim 50\text{--}300$ K between the T_{eff} scales of the Sun and the spectroscopic surveys studied here could place the Sun on the long-period pile-up. If the Sun has evolved through the pile-up, there is

some modest tension with the Sun’s age and the ages of the oldest stars on the pile-up; some of the cooler long-period pile-up stars in the CKS sample are both more massive and older than the Sun, which contradicts the expectation from the WMB model that hotter stars spend a shorter period of time on the pile-up. However, this tension might be simply explained by inaccurate isochrone ages.

5. We **tentatively detect** a secondary overdensity of stars at the short-period edge of the $T_{\text{eff}} - P_{\text{rot}}$ plane. This overdensity **appears to be** less prominent than the long-period overdensity, **possibly** because the short-period pile-up is shorter-lived ($\mathcal{O}(10^8 \text{ yr})$) relative to the long-period pile-up ($> 10^9 \text{ yr}$). The short-period pile-up appears to be intermediate to the empirical Pleiades (0.12 Gyr) and Praesepe (0.67 Gyr) open cluster sequences and may result from a temporary epoch of stalled spin-down due to core–envelope coupling, as proposed by Curtis et al. (2020). The short-period pile-up can also be fit with a constant Rossby model, though over a range of T_{eff} that differs from that of the long-period pile-up.
6. The number density of stars on the long-period pile-up declines with T_{eff} , in line with predictions from the WMB hypothesis, though it remains unclear whether this observation is due to astrophysics, the Kepler selection function, observational biases, or some combination of effects. The relative fraction of stars on the long-period pile up declines by a factor of ~ 2 between ~ 6200 K and ~ 5800 K.

7. We find tentative evidence for an age-gradient along the long-period pile-up, such that hotter stars on the ridge are younger on average. Relatedly, the age dispersion along the ridge is non-uniform as a function of temperature, with hotter stars showing a smaller dispersion. This observation suggests that hotter stars reside on the long-period pile-up for a shorter period of time relative to cooler stars. These observations are in accordance with predictions from the WMB model, which predicts that stars of different masses spend an approximately equal fraction of their respective main-sequence lifetimes on the long-period pile-up. However, a more careful analysis is required to conclusively show these observations are not due to the intrinsic age gradient expected among a sample of main sequence stars with different masses and the higher isochrone age uncertainties associated with cooler stars.
8. The existence of the long-period pile-up limits the utility of gyrochronology for the hottest stars with convective envelopes, as stellar spin-down appears to stall on the pile-up. For example, a Sun-like star may spend several Gyr evolving through the long-period pile-up. Authors using gyrochronology as a means of age-dating a field dwarf star with $T_{\text{eff}} \gtrsim 5500$ K (and possibly cooler T_{eff} as

well) should take care to assess whether that star resides on the long-period edge, in which case the uncertainty on the age may be larger than current gyrochronology calibrations imply.

9. An increasing number of open clusters are being discovered by searching for a clustering of rotation periods along a slow-rotator sequence in the $T_{\text{eff}} - P_{\text{rot}}$ or color- P_{rot} plane. However, the long-period pile up discovered here can mimic a slow-rotator sequence in a small sample of unassociated stars with different ages and precisely measured temperatures and rotation periods. This is clearly demonstrated by the CKS sample in the right-hand panel of Figure 1. Taken out of context, this sample resembles a group of coeval stars with a slow-rotator sequence. The discovery of pile-ups in stellar rotation periods therefore has consequences for open cluster studies. When an overdensity or ridge is present in the rotation period distribution of a stellar population, care must be taken to ensure that it is not caused by WMB or core-envelope coupling before assuming that population is coeval and using the overdensity to age-date it.

The code and data tables required to reproduce the figures and analysis presented here are publicly available through GitHub.⁵

APPENDIX

A. COMPARISON OF TEMPERATURE-PERIOD DISTRIBUTIONS

In Figure 14, we show how the $T_{\text{eff}} - P_{\text{rot}}$ distribution of the CKS sample changes when sourcing T_{eff} and P_{rot} from different, homogeneous catalogs in the literature. The sharpness of the long-period pile-up appears to be determined primarily by the source of T_{eff} , rather than P_{rot} . The CKS-Gaia catalog (Fulton & Petigura 2018) appears to offer the highest internal precision.

B. COMPARISON OF SPECTROSCOPIC TEMPERATURE SCALES

In Figure 16 we compare temperatures between the **LAMOST DR5** catalog (Xiang et al. 2019) and temperatures from other surveys. We find that the LAMOST T_{eff} scale is consistently cooler than other surveys by ~ 20 – 80 K, with the exception of the McQuillan et al. (2014) study which sourced photometric T_{eff} estimates from the KIC (Brown et al. 2011). A LAMOST T_{eff} scale which is systematically cooler provides support to the notion that R_{crit} determined from LAMOST temperatures will be systematically underestimated.

⁵ <https://github.com/trevordavid/rossby-ridge>

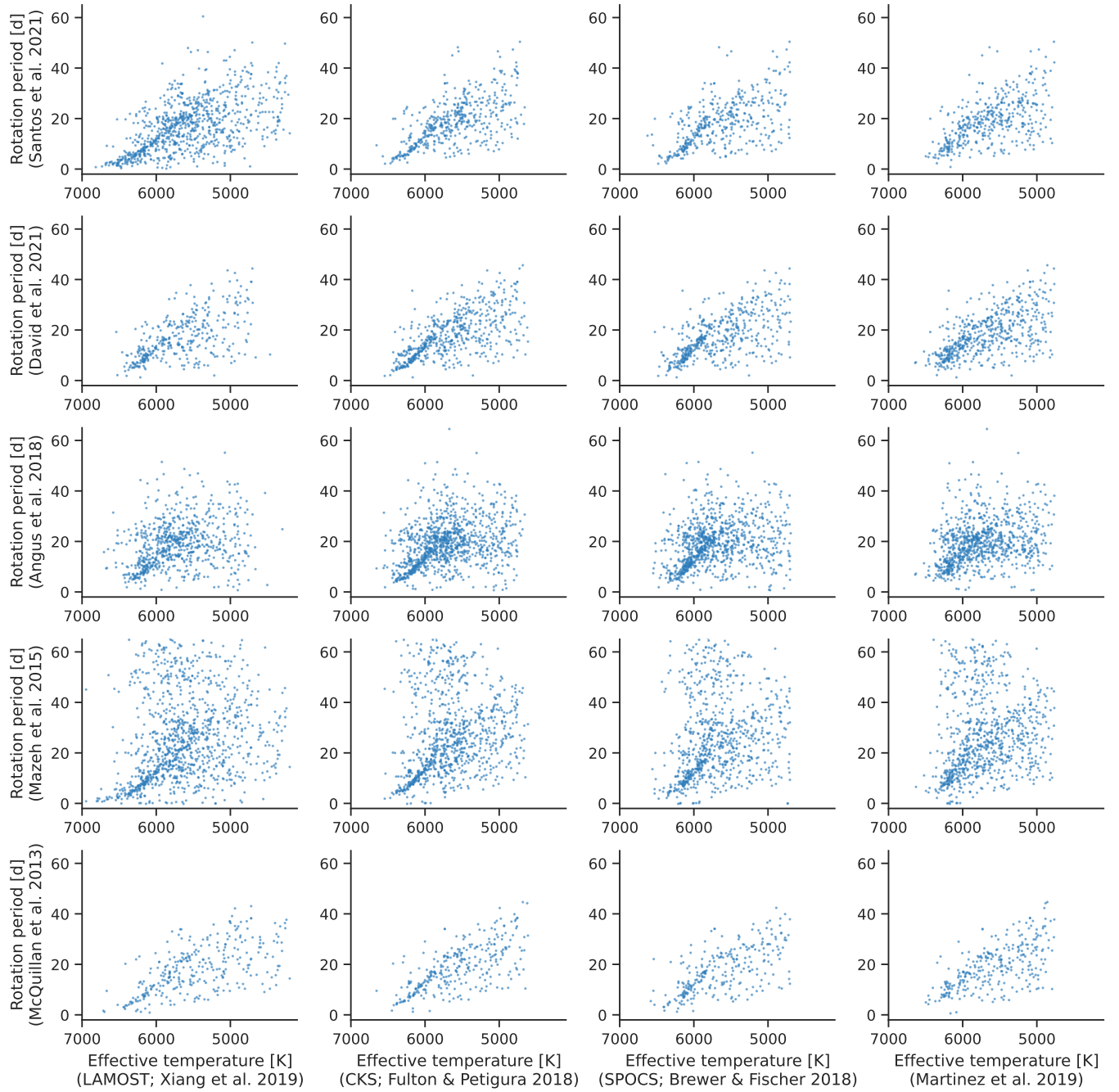


Figure 14. Comparison of the $T_{\text{eff}} - P_{\text{rot}}$ distribution for the CKS sample using rotation periods and T_{eff} from the sources indicated by the axes labels.



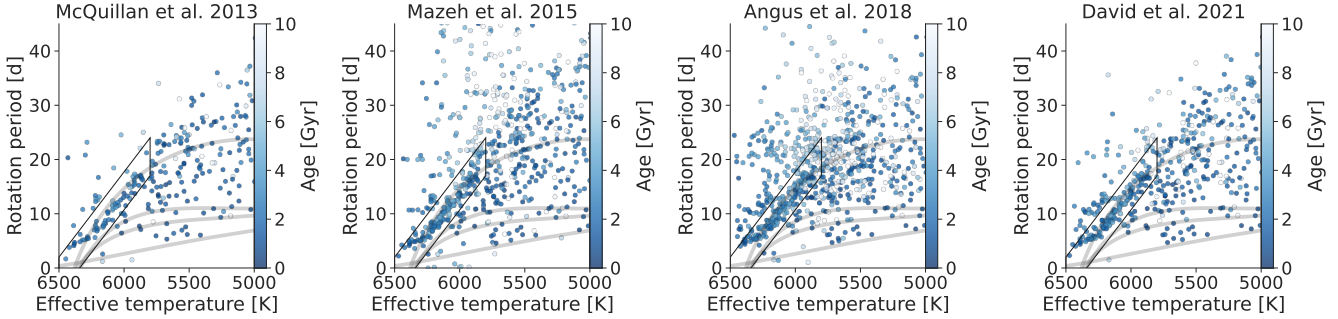


Figure 15. The $T_{\text{eff}}-P_{\text{rot}}$ plane for the CKS sample. Point colors are scaled to the CKS ages determined from isochrone fitting. The source of P_{rot} is denoted above each panel, where David et al. (2021) is a compilation of vetted periods, rather than a source of original measurements. The black trapezoid indicates the approximate area of the ridge. The grey curves indicate empirical cluster sequences from Curtis et al. (2020), corresponding to ages of $\sim 2.7, 1, 0.67$, and 0.12 Gyr from top to bottom.

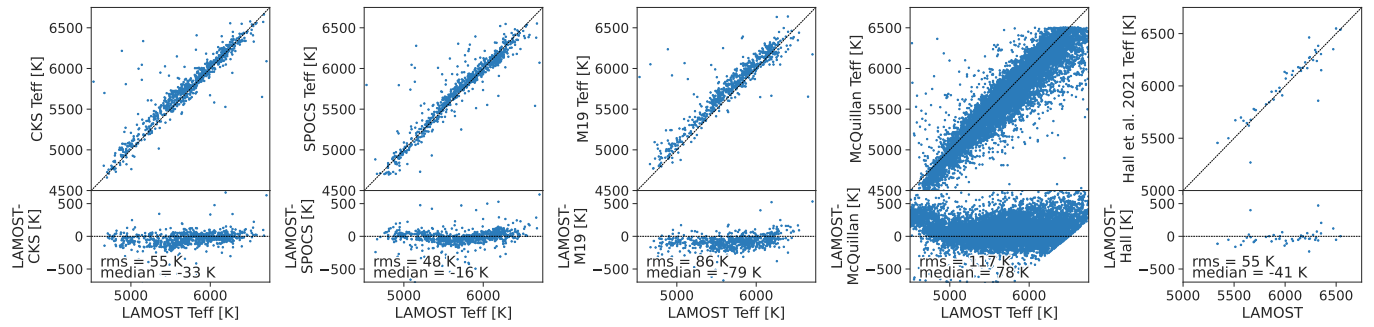


Figure 16. Comparison of T_{eff} estimates from different catalogs: LAMOST (Xiang et al. 2019), CKS (Fulton & Petigura 2018), SPOCS (Brewer & Fischer 2018), M19 (Martinez et al. 2019), McQuillan et al. (2014), and Hall et al. (2021).



1 We thank the anonymous referee for a thoughtful review, Rodrigo Luger for helpful discussions and assistance with
 2 the `showyourwork!` package, Adrian Price-Whelan for providing the APOGEE–Kepler cross-match catalog, and Karl
 3 Jaehnig for plotting advice. It is a pleasure to thank the Stars Group at the American Museum of Natural History,
 4 and the Astronomical Data Group at the Flatiron Institute for helpful discussions.

5 This work made use of the `gaia-kepler.fun` crossmatch database created by Megan Bedell. This paper includes data
 6 collected by the Kepler mission and obtained from the MAST data archive at the Space Telescope Science Institute
 7 (STScI).

8 Funding for the Kepler mission is provided by the NASA Science Mission Directorate. STScI is operated by the
 9 Association of Universities for Research in Astronomy, Inc., under NASA contract NAS 5–26555.

10 Guoshoujing Telescope (the Large Sky Area Multi-Object Fiber Spectroscopic Telescope LAMOST) is a National
 11 Major Scientific Project built by the Chinese Academy of Sciences. Funding for the project has been provided by the
 12 National Development and Reform Commission. LAMOST is operated and managed by the National Astronomical
 13 Observatories, Chinese Academy of Sciences.

14 This work has made use of data from the European Space Agency (ESA) mission *Gaia* (<https://www.cosmos.esa.int/gaia>), processed by the *Gaia* Data Processing and Analysis Consortium (DPAC, <https://www.cosmos.esa.int/web/gaia/dpac/consortium>). Funding for the DPAC has been provided by national institutions, in particular the
 15 institutions participating in the *Gaia* Multilateral Agreement.

16 Funding for the Sloan Digital Sky Survey IV has been provided by the Alfred P. Sloan Foundation, the U.S. Department
 17 of Energy Office of Science, and the Participating Institutions. SDSS-IV acknowledges support and resources
 18 from the Center for High Performance Computing at the University of Utah. The SDSS website is www.sdss.org.
 19 SDSS-IV is managed by the Astrophysical Research Consortium for the Participating Institutions of the SDSS Collaboration
 20 including the Brazilian Participation Group, the Carnegie Institution for Science, Carnegie Mellon University,
 21 Center for Astrophysics | Harvard & Smithsonian, the Chilean Participation Group, the French Participation Group,
 22 Instituto de Astrofísica de Canarias, The Johns Hopkins University, Kavli Institute for the Physics and Mathematics
 23 of the Universe (IPMU) / University of Tokyo, the Korean Participation Group, Lawrence Berkeley National Laboratory,
 24 Leibniz Institut für Astrophysik Potsdam (AIP), Max-Planck-Institut für Astronomie (MPIA Heidelberg),
 25 Max-Planck-Institut für Astrophysik (MPA Garching), Max-Planck-Institut für Extraterrestrische Physik (MPE), National
 26 Astronomical Observatories of China, New Mexico State University, New York University, University of Notre Dame,
 27 Observatório Nacional / MCTI, The Ohio State University, Pennsylvania State University, Shanghai Astronomical
 28 Observatory, United Kingdom Participation Group, Universidad Nacional Autónoma de México, University
 29 of Arizona, University of Colorado Boulder, University of Oxford, University of Portsmouth, University of Utah,
 30 University of Virginia, University of Washington, University of Wisconsin, Vanderbilt University, and Yale University.
 31

32 This research has made use of NASA’s Astrophysics Data System Bibliographic Services.

Facilities: Gaia; Kepler; Keck:I (HIRES); LAMOST; Sloan (APOGEE)

Software: `astropy` (Astropy Collaboration et al. 2013, 2018), `corner` (Foreman-Mackey 2016), `emcee` (Foreman-Mackey et al. 2013, 2019), `jupyter` (Kluyver et al. 2016), `matplotlib` (Hunter 2007), `numpy` (van der Walt et al. 2011), `pandas` (pandas development team 2020; Wes McKinney 2010), `scipy` (Jones et al. 2001–), `seaborn` (Waskom et al. 2017), `showyourwork!` (Luger et al. 2021)

REFERENCES

- Agüeros, M. A., Bowsher, E. C., Bochanski, J. J., et al. 2018, ApJ, 862, 33, doi: [10.3847/1538-4357/aac6ed](https://doi.org/10.3847/1538-4357/aac6ed)
- Ahumada, R., Prieto, C. A., Almeida, A., et al. 2020, ApJS, 249, 3, doi: [10.3847/1538-4365/ab929e](https://doi.org/10.3847/1538-4365/ab929e)
- Aigrain, S., Llama, J., Ceillier, T., et al. 2015, MNRAS, 450, 3211, doi: [10.1093/mnras/stv853](https://doi.org/10.1093/mnras/stv853)
- Angus, R., Aigrain, S., Foreman-Mackey, D., & McQuillan, A. 2015, MNRAS, 450, 1787, doi: [10.1093/mnras/stv423](https://doi.org/10.1093/mnras/stv423)
- Angus, R., Morton, T., Aigrain, S., Foreman-Mackey, D., & Rajpaul, V. 2018, MNRAS, 474, 2094, doi: [10.1093/mnras/stx2109](https://doi.org/10.1093/mnras/stx2109)
- Astropy Collaboration, Robitaille, T. P., Tollerud, E. J., et al. 2013, A&A, 558, A33, doi: [10.1051/0004-6361/201322068](https://doi.org/10.1051/0004-6361/201322068)

- Astropy Collaboration, Price-Whelan, A. M., SipH ocz, B. M., et al. 2018, AJ, 156, 123, doi: [10.3847/1538-3881/aabc4f](https://doi.org/10.3847/1538-3881/aabc4f)
- Bahcall, J. N., Pinsonneault, M. H., & Wasserburg, G. J. 1995, Reviews of Modern Physics, 67, 781, doi: [10.1103/RevModPhys.67.781](https://doi.org/10.1103/RevModPhys.67.781)
- Barnes, S. A. 2003, ApJ, 586, 464, doi: [10.1086/367639](https://doi.org/10.1086/367639)
- . 2007, ApJ, 669, 1167, doi: [10.1086/519295](https://doi.org/10.1086/519295)
- . 2010, ApJ, 722, 222, doi: [10.1088/0004-637X/722/1/222](https://doi.org/10.1088/0004-637X/722/1/222)
- Barnes, S. A., & Kim, Y.-C. 2010, ApJ, 721, 675, doi: [10.1088/0004-637X/721/1/675](https://doi.org/10.1088/0004-637X/721/1/675)
- Blanton, M. R., Bershadsky, M. A., Abolfathi, B., et al. 2017, AJ, 154, 28, doi: [10.3847/1538-3881/aa7567](https://doi.org/10.3847/1538-3881/aa7567)
- Borucki, W. J., Koch, D., Basri, G., et al. 2010, Science, 327, 977, doi: [10.1126/science.1185402](https://doi.org/10.1126/science.1185402)
- Bouvier, J. 2008, A&A, 489, L53, doi: [10.1051/0004-6361:200810574](https://doi.org/10.1051/0004-6361:200810574)
- Brewer, J. M., & Fischer, D. A. 2018, ApJS, 237, 38, doi: [10.3847/1538-4365/aad501](https://doi.org/10.3847/1538-4365/aad501)
- Brown, T. M., Latham, D. W., Everett, M. E., & Esquerdo, G. A. 2011, AJ, 142, 112, doi: [10.1088/0004-6256/142/4/112](https://doi.org/10.1088/0004-6256/142/4/112)
- Cranmer, S. R., & Saar, S. H. 2011, ApJ, 741, 54, doi: [10.1088/0004-637X/741/1/54](https://doi.org/10.1088/0004-637X/741/1/54)
- Curtis, J. L., Agüeros, M. A., Douglas, S. T., & Meibom, S. 2019a, ApJ, 879, 49, doi: [10.3847/1538-4357/ab2393](https://doi.org/10.3847/1538-4357/ab2393)
- Curtis, J. L., Agüeros, M. A., Mamajek, E. E., Wright, J. T., & Cummings, J. D. 2019b, AJ, 158, 77, doi: [10.3847/1538-3881/ab2899](https://doi.org/10.3847/1538-3881/ab2899)
- Curtis, J. L., Agüeros, M. A., Matt, S. P., et al. 2020, ApJ, 904, 140, doi: [10.3847/1538-4357/abbf58](https://doi.org/10.3847/1538-4357/abbf58)
- Davenport, J. R. A. 2017, ApJ, 835, 16, doi: [10.3847/1538-4357/835/1/16](https://doi.org/10.3847/1538-4357/835/1/16)
- Davenport, J. R. A., & Covey, K. R. 2018, ApJ, 868, 151, doi: [10.3847/1538-4357/aae842](https://doi.org/10.3847/1538-4357/aae842)
- David, T. J., Contardo, G., Sandoval, A., et al. 2021, AJ, 161, 265, doi: [10.3847/1538-3881/abf439](https://doi.org/10.3847/1538-3881/abf439)
- Denissenkov, P. A., Pinsonneault, M., Terndrup, D. M., & Newsham, G. 2010, ApJ, 716, 1269, doi: [10.1088/0004-637X/716/2/1269](https://doi.org/10.1088/0004-637X/716/2/1269)
- Douglas, S. T., Agüeros, M. A., Covey, K. R., et al. 2016, ApJ, 822, 47, doi: [10.3847/0004-637X/822/1/47](https://doi.org/10.3847/0004-637X/822/1/47)
- Douglas, S. T., Agüeros, M. A., Covey, K. R., & Kraus, A. 2017, ApJ, 842, 83, doi: [10.3847/1538-4357/aa6e52](https://doi.org/10.3847/1538-4357/aa6e52)
- Douglas, S. T., Curtis, J. L., Agüeros, M. A., et al. 2019, ApJ, 879, 100, doi: [10.3847/1538-4357/ab2468](https://doi.org/10.3847/1538-4357/ab2468)
- Dressing, C. D., & Charbonneau, D. 2013, ApJ, 767, 95, doi: [10.1088/0004-637X/767/1/95](https://doi.org/10.1088/0004-637X/767/1/95)
- Foreman-Mackey, D. 2016, The Journal of Open Source Software, 1, 24, doi: [10.21105/joss.00024](https://doi.org/10.21105/joss.00024)
- Foreman-Mackey, D., Hogg, D. W., Lang, D., & Goodman, J. 2013, PASP, 125, 306, doi: [10.1086/670067](https://doi.org/10.1086/670067)
- Foreman-Mackey, D., Farr, W., Sinha, M., et al. 2019, The Journal of Open Source Software, 4, 1864, doi: [10.21105/joss.01864](https://doi.org/10.21105/joss.01864)
- Fulton, B. J., & Petigura, E. A. 2018, AJ, 156, 264, doi: [10.3847/1538-3881/aae828](https://doi.org/10.3847/1538-3881/aae828)
- Gaia Collaboration, Prusti, T., de Bruijne, J. H. J., et al. 2016, A&A, 595, A1, doi: [10.1051/0004-6361/201629272](https://doi.org/10.1051/0004-6361/201629272)
- Gaia Collaboration, Brown, A. G. A., Vallenari, A., et al. 2018, A&A, 616, A1, doi: [10.1051/0004-6361/201833051](https://doi.org/10.1051/0004-6361/201833051)
- Gallet, F., & Bouvier, J. 2015, A&A, 577, A98, doi: [10.1051/0004-6361/201525660](https://doi.org/10.1051/0004-6361/201525660)
- Garraffo, C., Drake, J. J., & Cohen, O. 2016, A&A, 595, A110, doi: [10.1051/0004-6361/201628367](https://doi.org/10.1051/0004-6361/201628367)
- Gordon, T. A., Davenport, J. R. A., Angus, R., et al. 2021, ApJ, 913, 70, doi: [10.3847/1538-4357/abf63e](https://doi.org/10.3847/1538-4357/abf63e)
- Gunn, A. G., Mitrou, C. K., & Doyle, J. G. 1998, MNRAS, 296, 150, doi: [10.1046/j.1365-8711.1998.01347.x](https://doi.org/10.1046/j.1365-8711.1998.01347.x)
- Hall, O. J., Davies, G. R., van Sadlers, J., et al. 2021, Nature Astronomy, 5, 707, doi: [10.1038/s41550-021-01335-x](https://doi.org/10.1038/s41550-021-01335-x)
- Howell, S. B., Sobeck, C., Haas, M., et al. 2014, PASP, 126, 398, doi: [10.1086/676406](https://doi.org/10.1086/676406)
- Huber, D., Silva Aguirre, V., Matthews, J. M., et al. 2014, ApJS, 211, 2, doi: [10.1088/0067-0049/211/1/2](https://doi.org/10.1088/0067-0049/211/1/2)
- Hunter, J. D. 2007, Computing in Science and Engineering, 9, 90, doi: [10.1109/MCSE.2007.55](https://doi.org/10.1109/MCSE.2007.55)
- Irwin, J., & Bouvier, J. 2009, in The Ages of Stars, ed. E. E. Mamajek, D. R. Soderblom, & R. F. G. Wyse, Vol. 258, 363–374, doi: [10.1017/S1743921309032025](https://doi.org/10.1017/S1743921309032025)
- Irwin, J., Hodgkin, S., Aigrain, S., et al. 2007, MNRAS, 377, 741, doi: [10.1111/j.1365-2966.2007.11640.x](https://doi.org/10.1111/j.1365-2966.2007.11640.x)
- Jones, E., Oliphant, T., Peterson, P., et al. 2001–, SciPy: Open source scientific tools for Python. <http://www.scipy.org/>
- Jönsson, H., Holtzman, J. A., Allende Prieto, C., et al. 2020, AJ, 160, 120, doi: [10.3847/1538-3881/aba592](https://doi.org/10.3847/1538-3881/aba592)
- Kawaler, S. D. 1988, ApJ, 333, 236, doi: [10.1086/166740](https://doi.org/10.1086/166740)
- Kluyver, T., Ragan-Kelley, B., Pérez, F., et al. 2016, in Positioning and Power in Academic Publishing: Players, Agents and Agendas, ed. F. Loizides & B. Schmidt, IOS Press, 87 – 90
- Kraft, R. P. 1967, ApJ, 150, 551, doi: [10.1086/149359](https://doi.org/10.1086/149359)
- Krishnamurthi, A., Pinsonneault, M. H., Barnes, S., & Sofia, S. 1997, ApJ, 480, 303, doi: [10.1086/303958](https://doi.org/10.1086/303958)
- Landin, N. R., Mendes, L. T. S., & Vaz, L. P. R. 2010, A&A, 510, A46, doi: [10.1051/0004-6361/200913015](https://doi.org/10.1051/0004-6361/200913015)
- Lanzafame, A. C., & Spada, F. 2015, A&A, 584, A30, doi: [10.1051/0004-6361/201526770](https://doi.org/10.1051/0004-6361/201526770)

- Lorenzo-Oliveira, D., Meléndez, J., Ponte, G., & Galarza, J. Y. 2020, MNRAS, 495, L61, doi: [10.1093/mnrasl/slaa057](https://doi.org/10.1093/mnrasl/slaa057)
- Lorenzo-Oliveira, D., Meléndez, J., Yana Galarza, J., et al. 2019, MNRAS, 485, L68, doi: [10.1093/mnrasl/slz034](https://doi.org/10.1093/mnrasl/slz034)
- Luger, R., Bedell, M., Foreman-Mackey, D., et al. 2021, arXiv e-prints, arXiv:2110.06271. <https://arxiv.org/abs/2110.06271>
- MacGregor, K. B., & Brenner, M. 1991, ApJ, 376, 204, doi: [10.1086/170269](https://doi.org/10.1086/170269)
- Majewski, S. R., Schiavon, R. P., Frinchaboy, P. M., et al. 2017, AJ, 154, 94, doi: [10.3847/1538-3881/aa784d](https://doi.org/10.3847/1538-3881/aa784d)
- Mamajek, E. E., & Hillenbrand, L. A. 2008, ApJ, 687, 1264, doi: [10.1086/591785](https://doi.org/10.1086/591785)
- Martinez, C. F., Cunha, K., Ghezzi, L., & Smith, V. V. 2019, ApJ, 875, 29, doi: [10.3847/1538-4357/ab0d93](https://doi.org/10.3847/1538-4357/ab0d93)
- Masuda, K., Petigura, E. A., & Hall, O. J. 2021, arXiv e-prints, arXiv:2112.07162. <https://arxiv.org/abs/2112.07162>
- Mazeh, T., Perets, H. B., McQuillan, A., & Goldstein, E. S. 2015, ApJ, 801, 3, doi: [10.1088/0004-637X/801/1/3](https://doi.org/10.1088/0004-637X/801/1/3)
- McQuillan, A., Aigrain, S., & Mazeh, T. 2013a, MNRAS, 432, 1203, doi: [10.1093/mnras/stt536](https://doi.org/10.1093/mnras/stt536)
- McQuillan, A., Mazeh, T., & Aigrain, S. 2013b, ApJL, 775, L11, doi: [10.1088/2041-8205/775/1/L11](https://doi.org/10.1088/2041-8205/775/1/L11)
- . 2014, ApJS, 211, 24, doi: [10.1088/0067-0049/211/2/24](https://doi.org/10.1088/0067-0049/211/2/24)
- Meibom, S., Barnes, S. A., Platais, I., et al. 2015, Nature, 517, 589, doi: [10.1038/nature14118](https://doi.org/10.1038/nature14118)
- Meibom, S., Mathieu, R. D., & Stassun, K. G. 2009, ApJ, 695, 679, doi: [10.1088/0004-637X/695/1/679](https://doi.org/10.1088/0004-637X/695/1/679)
- Meibom, S., Barnes, S. A., Latham, D. W., et al. 2011, ApJL, 733, L9, doi: [10.1088/2041-8205/733/1/L9](https://doi.org/10.1088/2041-8205/733/1/L9)
- Mestel, L. 1968, MNRAS, 138, 359, doi: [10.1093/mnras/138.3.359](https://doi.org/10.1093/mnras/138.3.359)
- Metcalfe, T. S., Egeland, R., & van Saders, J. 2016, ApJL, 826, L2, doi: [10.3847/2041-8205/826/1/L2](https://doi.org/10.3847/2041-8205/826/1/L2)
- Metcalfe, T. S., Kochukhov, O., Ilyin, I. V., et al. 2019, ApJL, 887, L38, doi: [10.3847/2041-8213/ab5e48](https://doi.org/10.3847/2041-8213/ab5e48)
- Ness, M., Hogg, D. W., Rix, H. W., Ho, A. Y. Q., & Zasowski, G. 2015, ApJ, 808, 16, doi: [10.1088/0004-637X/808/1/16](https://doi.org/10.1088/0004-637X/808/1/16)
- pandas development team, T. 2020, pandas-dev/pandas: Pandas, latest, Zenodo, doi: [10.5281/zenodo.3509134](https://doi.org/10.5281/zenodo.3509134)
- Parker, E. N. 1958, ApJ, 128, 664, doi: [10.1086/146579](https://doi.org/10.1086/146579)
- Petigura, E. A. 2015, PhD thesis, University of California, Berkeley
- Petigura, E. A., Howard, A. W., Marcy, G. W., et al. 2017, AJ, 154, 107, doi: [10.3847/1538-3881/aa80de](https://doi.org/10.3847/1538-3881/aa80de)
- Prša, A., Harmanec, P., Torres, G., et al. 2016, AJ, 152, 41, doi: [10.3847/0004-6256/152/2/41](https://doi.org/10.3847/0004-6256/152/2/41)
- Rebull, L. M., Stauffer, J. R., Cody, A. M., et al. 2020, AJ, 159, 273, doi: [10.3847/1538-3881/ab893c](https://doi.org/10.3847/1538-3881/ab893c)
- . 2018, AJ, 155, 196, doi: [10.3847/1538-3881/aab605](https://doi.org/10.3847/1538-3881/aab605)
- Rebull, L. M., Stauffer, J. R., Hillenbrand, L. A., et al. 2017, ApJ, 839, 92, doi: [10.3847/1538-4357/aa6aaa4](https://doi.org/10.3847/1538-4357/aa6aaa4)
- Rebull, L. M., Stauffer, J. R., Bouvier, J., et al. 2016, AJ, 152, 113, doi: [10.3847/0004-6256/152/5/113](https://doi.org/10.3847/0004-6256/152/5/113)
- Reinhold, T., Bell, K. J., Kuszlewicz, J., Hekker, S., & Shapiro, A. I. 2019, A&A, 621, A21, doi: [10.1051/0004-6361/201833754](https://doi.org/10.1051/0004-6361/201833754)
- Reinhold, T., & Hekker, S. 2020, A&A, 635, A43, doi: [10.1051/0004-6361/201936887](https://doi.org/10.1051/0004-6361/201936887)
- Reinhold, T., Reiners, A., & Basri, G. 2013, A&A, 560, A4, doi: [10.1051/0004-6361/201321970](https://doi.org/10.1051/0004-6361/201321970)
- Réville, V., Brun, A. S., Matt, S. P., Strugarek, A., & Pinto, R. F. 2015, ApJ, 798, 116, doi: [10.1088/0004-637X/798/2/116](https://doi.org/10.1088/0004-637X/798/2/116)
- Ricker, G. R., Winn, J. N., Vanderspek, R., et al. 2015, Journal of Astronomical Telescopes, Instruments, and Systems, 1, 014003, doi: [10.1117/1.JATIS.1.1.014003](https://doi.org/10.1117/1.JATIS.1.1.014003)
- Santos, A. R. G., Breton, S. N., Mathur, S., & García, R. A. 2021, ApJS, 255, 17, doi: [10.3847/1538-4365/ac033f](https://doi.org/10.3847/1538-4365/ac033f)
- Skumanich, A. 1972, ApJ, 171, 565, doi: [10.1086/151310](https://doi.org/10.1086/151310)
- Somers, G., & Pinsonneault, M. H. 2016, ApJ, 829, 32, doi: [10.3847/0004-637X/829/1/32](https://doi.org/10.3847/0004-637X/829/1/32)
- Spada, F., & Lanzaafame, A. C. 2020, A&A, 636, A76, doi: [10.1051/0004-6361/201936384](https://doi.org/10.1051/0004-6361/201936384)
- Thompson, M. J., Christensen-Dalsgaard, J., Miesch, M. S., & Toomre, J. 2003, ARA&A, 41, 599, doi: [10.1146/annurev.astro.41.011802.094848](https://doi.org/10.1146/annurev.astro.41.011802.094848)
- Ting, Y.-S., Rix, H.-W., Conroy, C., Ho, A. Y. Q., & Lin, J. 2017, ApJL, 849, L9, doi: [10.3847/2041-8213/aa921c](https://doi.org/10.3847/2041-8213/aa921c)
- Valenti, J. A., & Piskunov, N. 1996, A&AS, 118, 595
- van der Walt, S., Colbert, S. C., & Varoquaux, G. 2011, Computing in Science and Engineering, 13, 22, doi: [10.1109/MCSE.2011.37](https://doi.org/10.1109/MCSE.2011.37)
- van Saders, J. L., Ceillier, T., Metcalfe, T. S., et al. 2016, Nature, 529, 181, doi: [10.1038/nature16168](https://doi.org/10.1038/nature16168)
- van Saders, J. L., & Pinsonneault, M. H. 2013, ApJ, 776, 67, doi: [10.1088/0004-637X/776/2/67](https://doi.org/10.1088/0004-637X/776/2/67)
- van Saders, J. L., Pinsonneault, M. H., & Barbieri, M. 2019, ApJ, 872, 128, doi: [10.3847/1538-4357/aaafae](https://doi.org/10.3847/1538-4357/aaafae)
- Vogt, S. S., Allen, S. L., Bigelow, B. C., et al. 1994, in Society of Photo-Optical Instrumentation Engineers (SPIE) Conference Series, Vol. 2198, Instrumentation in Astronomy VIII, ed. D. L. Crawford & E. R. Craine, 362, doi: [10.1117/12.176725](https://doi.org/10.1117/12.176725)
- Waskom, M., Botvinnik, O., O’Kane, D., et al. 2017, mwaskom/seaborn: v0.8.1 (September 2017), v0.8.1, Zenodo, doi: [10.5281/zenodo.883859](https://doi.org/10.5281/zenodo.883859)

- Weber, E. J., & Davis, Leverett, J. 1967, ApJ, 148, 217,
doi: [10.1086/149138](https://doi.org/10.1086/149138)
- Wes McKinney. 2010, in Proceedings of the 9th Python in
Science Conference, ed. Stéfan van der Walt & Jarrod
Millman, 56 – 61, doi: [10.25080/Majora-92bf1922-00a](https://doi.org/10.25080/Majora-92bf1922-00a)
- Xiang, M., Ting, Y.-S., Rix, H.-W., et al. 2019, ApJS, 245,
34, doi: [10.3847/1538-4365/ab5364](https://doi.org/10.3847/1538-4365/ab5364)
- Zong, W., Fu, J.-N., De Cat, P., et al. 2018, ApJS, 238, 30,
doi: [10.3847/1538-4365/aadf81](https://doi.org/10.3847/1538-4365/aadf81)